Experimental investigation into the impact of density wave oscillations on flow boiling system dynamic behavior and stability

Lucas E. O'Neill [a], Issam Mudawar [a,*], Mohammad M. Hasan [b], Henry K. Nahra [b], R. Balasubramaniam [b], Nancy R. Hall [b], Aubrey Lokey [b], Jeffery R. Mackey [c]

[a] Purdue University Boiling and Two-Phase Flow Laboratory (PU-BTPFL), School of Mechanical Engineering, Purdue University, 585 Purdue Mall, West Lafayette, IN 47907, USA
[b] NASA Glenn Research Center, 21000 Brookpark Road, Cleveland, OH 44135, USA
[c] Vantage Partners, 3000 Aerospace Parkway, Brook Park, OH 44142, USA

ARTICLE INFO

ABSTRACT

In order to better understand and quantify the effect of instabilities in systems utilizing flow boiling heat transfer, the present study explores dynamic results for pressure drop, mass velocity, thermodynamic equilibrium quality, and heated wall temperature to ascertain and analyze the dominant modes in which they oscillate. Flow boiling experiments are conducted for a range of mass velocities with both subcooled and saturated inlet conditions in vertical upflow, vertical downflow, and horizontal flow orientations. High frequency pressure measurements are used to investigate the influence of individual flow loop components (flow boiling module, pump, pre-heater, condenser, *etc.*) on dynamic behavior of the fluid, with fast Fourier transforms of the same used to provide critical frequency domain information. Conclusions from this analysis are used to isolate instabilities present within the system due to physical interplay between thermodynamic and hydrodynamic effects. Parametric analysis is undertaken to better understand the conditions under which these instabilities form and their impact on system performance. Several prior stability maps are presented, with new stability maps provided to better address contextual trends discovered in the present study.

© 2017 Elsevier Ltd. All rights reserved.

1. Introduction

1.1. Challenges limiting the adoption of two-phase thermal management systems

Across industries worldwide, thermal design engineers are turning to phase change energy transfer methods to meet increasingly difficult thermal management requirements posed by successive generations of products [1]. By using boiling for device cooling and condensation for heat rejection, both latent and sensible heat of the fluid can be utilized, allowing achievement of orders of magnitude improvement in heat transfer compared to traditional single-phase alternatives.

Although useful for any application involving thermal management of high energy density devices, phase change systems show particular promise in the field of space thermal-fluid systems, where their high heat transfer coefficients can allow an appreciable reduction in size and weight of hardware. Because of this potential, space agencies worldwide are investigating the benefits and drawbacks accompanying implementation of two-phase systems in both space vehicles and planetary bases. Current targets for adoption of phase change technologies include Thermal Control Systems (TCSs), which control temperature and humidity of the operating environment, heat receiver and heat rejection systems for power generating units, and Fission Power Systems (FPSs), which are projected to provide high power as well as low mass to power ratio [2–4].

Unlike their Earth-based counterparts, however, use of two-phase cooling schemes for space missions entails the added complication of variable body force across missions or even across mission duration. From hyper-gravity associated with launch, to microgravity encountered in interplanetary transit and orbit, to unique planetary gravitational accelerations, thermal management systems designed to operate in space must be robust enough to perform in a broad range of gravitational accelerations. This greatly complicates the use of two-phase thermal management systems, where the orders of magnitude density difference between phases causes body force (buoyancy) effects to impact flow behavior significantly. To adequately mitigate the risks associated with operation in space, accurate, robust design tools for a wide array of boiling configurations is a necessity.

---

* Corresponding author.
  E-mail address: mudawar@ecn.purdue.edu (I. Mudawar).
  URL: https://engineering.purdue.edu/BTPFL (I. Mudawar).

Nomenclature

A	amplitude		T_{sat}	saturation temperature
c_p	specific heat at constant pressure		$T_{sat,in}$	saturation temperature of fluid at inlet to heated portion of channel
D_h	hydraulic diameter			
f	frequency		T_{tr}	transport time
f_r	resonant frequency		U	mean velocity
G	mass velocity		v	specific volume
H	height of flow channel's cross-section		W	width of flow channel's cross-section
h_{fg}	latent heat of vaporization		x	quality
L	length		x_e	thermodynamic equilibrium quality
L_d	development length of flow channel			
L_e	exit length of flow channel		*Greek symbol*	
L_h	heated length of flow channel		μ	dynamic viscosity
$\dot{m}$	mass flow rate			
N_{pch}	phase change number		*Subscripts*	
N_{sub}	subcooling number		*ave*	average
P	pressure		*exp*	experimental (measured)
ΔP	pressure drop across heated portion of channel		f	saturated liquid
P_{in}	pressure at inlet to heated portion of channel		*FBM*	flow boiling module
P_{out}	pressure at outlet to heated portion of channel		*FC*	FC-72 fluid
Pwr_{PH}	power supplied by pre-heater		g	saturated vapor
Q	total heat input		*in*	inlet to heated portion of channel
q''	heat flux on heated perimeter of channel		m	heated wall identifier (*a* for heater H_a or *b* for heater H_b)
Re	Reynolds number			
Re_f	superficial liquid Reynolds number, $Re_f = G(1-x)D_h/\mu_f$		*PH*	pre-heater
T	temperature		*pred*	predicted
t	time		*sat*	saturation
T_{in}	temperature at channel inlet		w	wall

Many previous studies have investigated a variety of schemes for heat acquisition through boiling, including pool boiling thermosyphons [5,6], falling film [7–9], channel flow boiling [10], micro-channel boiling [11,12], jet impingement [13–15], and spray [16–18], as well as hybrid configurations [19] involving two or more of these schemes. While each configuration possesses unique attributes as well as drawbacks, all suffer from a lack of understanding regarding the precise influence of body force on system performance, and transient system performance in particular.

Although most researchers and design engineers are primarily concerned with steady, time-averaged values for key parameters such as heat transfer coefficient, pressure drop, and critical heat flux (CHF), under certain conditions, system transient behavior has the ability to significantly impact performance and drive system design. These include operation near a critical point (*e.g.,* choking, CHF), where fluctuations in operating conditions brought on by instabilities inherent to flow boiling systems have the capacity to push the system into a failure mode, and applications concerned with precise system control (*e.g.,* maintaining science instrument temperature within a small range), where oscillations degrade system performance. Additionally, and of particular interest to the present study, is the case of changing body force (brought on by system utilization in space vehicles). As evidenced by previous studies conducted with the aid of parabolic flight [20,21], rapid changes in local acceleration lead to dynamic changes in flow boiling behavior. Better characterization of flow boiling transient behavior and the effects of body force variations on this behavior are crucial to designing the next generation of space-based thermal management systems.

1.2. Flow boiling instabilities and transient behavior

Due to the complex interplay of fluid and thermal effects, two-phase flows with mass transfer (flow boiling, flow condensation) commonly exhibit flow '*instabilities*', dynamic, transient events that can impact system performance under certain conditions. The study of two-phase flow instabilities originated with Ledinegg [22], who discovered that, under certain operating conditions, two-phase flow systems can experience an excursion from an unstable location to a stable location on the system's internal-external pressure curve, manifest as a change in mass velocity within the system.

It was not until several decades later that researchers began to delve into less noticeable, more persistent transient phenomena found in two-phase flow systems [23–25], with special attention paid to Density Wave Oscillations (DWOs) [26,27]. It was around the same time that Boure et al. published their seminal review of two-phase flow instabilities [28], which contains two facts of particular interest to the present work:

(1) Two-phase flow instabilities can be broadly classified into two groups: (a) '*static instabilities*', indicating a single excursion to a new operating condition (*e.g.,* Ledinegg instability, CHF), and (b) '*dynamic instabilities*', which are continuous, periodic oscillations within the flow (*e.g.,* DWOs, Pressure Drop Oscillations, Parallel Channel Instability).
(2) Instabilities falling into the second category of dynamic instabilities can often be best characterized by analyzing the frequencies at which they occur.

Recently, researchers have continued to focus on characterization of flow boiling transient behavior in a wide range of two-phase flow systems, including systems driven by natural circulation [29], forced flow in single mini-channels [30–32] and micro-channels [33,34], and in parallel micro-channel heat sinks [35–40]. Recent reviews, such as those by Tadrist [41], Kakac and Bon [42], and Ruspini et al. [43], provide updated surveys of literature relating to phenomena first reported by Boure et al. [28], including overviews of analytic, empiric, and numeric approaches adopted in modeling their behavior. From the lack of overlap

between experimental and analytical work, however, it is evident that further investigation is necessary to develop a better fundamental understanding of instabilities and accurately assess their impact on system performance.

1.3. Objectives of study

This study is part of a joint project between Purdue University Boiling and Two-Phase Flow Laboratory (PU-BTPFL) and NASA Glenn Research Center (GRC) whose ultimate goal is to develop the Flow Boiling and Condensation Experiment (FBCE) for the International Space Station (ISS). The current work deals with flow boiling, and aims to utilize experimental results gathered at multiple orientations with respect to Earth's gravity to heighten understanding of the impact of body force on system dynamic behavior and occurrence of key transient phenomena such as instabilities.

Flow boiling experiments are performed in a rectangular channel with both subcooled and saturated inlet conditions at three orientations in Earth's gravity: vertical upflow, vertical downflow, and horizontal flow. The channel features two opposite heated walls that can be operated independently, although in the present study tests were run with both walls heated.

Analysis of transient experimental results is undertaken with two key objectives:

(1) Determine the contribution of fluid machinery and fluid components on dynamic flow boiling behavior, so as to isolate the influence of physical phenomena that occur independent of fluid machinery and components in use.
(2) Having isolated transient, physical phenomena of interest, perform parametric evaluation of trends relative to changes in key parameters such as mass velocity, inlet conditions, heat flux, and orientation.

In an effort to complement previous studies conducted as part of the ongoing project between PU-BTPFL and NASA GRC dealing primarily with characterization and prediction of important time-averaged design parameters such as heat transfer coefficient [44–47], pressure drop [31,48–49], and CHF [50–53], the present study will also present and evaluate several flow boiling stability maps commonly found in literature.

2. Experimental methods

2.1. Flow boiling module

Part of FBCE intended for use on the ISS, the Flow Boiling Module (FBM) used in the present experiments is a test section designed to allow accurate heat transfer and pressure drop measurements while simultaneously facilitating capture of high-speed flow video imaging. The module is constructed from transparent polycarbonate plastic (Lexan) plates sandwiched between two aluminum support plates. As shown in Fig. 1(a), the central Lexan plate is milled out to create a rectangular 2.5-mm wide, 5-mm tall flow channel with a development length of 327.9 mm, followed by a heated length of 114.6 mm, and ending with a 60.9-mm exit length. Fig. 1(a) also shows the heated length is constructed by inserting oxygen-free copper slabs flush with the channel's top and bottom walls. Six 4.5-mm wide, 16.4-mm long, 188-Ω resistive heaters are soldered to the backs of the copper slabs, evenly spaced with small gaps between successive heaters to allow temperature measurements to be made using thermocouples. In the present study, equal heat flux is applied to both heated walls in all experiments.

Pressure measurements are made at five locations indicated in Fig. 1(b), including three along the development length, one upstream of the heated length, and one downstream of the heated length. Fig. 1(b) also shows the locations of inlet and outlet fluid temperature measurements, obtained with type-E thermocouples inserted directly into the flow.

Also illustrated in Fig. 1(b), heated wall temperatures are measured by seven evenly spaced type-E thermocouples per wall.

2.2. Flow boiling test loop

Desired inlet conditions for FBM are achieved using the flow loop shown schematically in Fig. 1(c) as well as in its physical form in Fig. 1(d). An Ismatech MCP-z magnetically-coupled gear pump is used to circulate the working fluid, FC-72, through the system. Exiting the pump, the fluid passes through a filter to remove any particulates from the flow before entering a turbine flow meter for flow rate measurement. After the flow meter, the fluid enters a 1500-W Cast-X pre-heater where power is supplied to set the fluid's thermodynamic conditions before it passes through a short insulated length of flexible tubing and enters the FBM. The FBM itself is mounted on a rotating stand to allow for quick changes to test section orientation without the need to reconfigure the flow loop.

Wall heat flux in the flow boiling module is controlled using the FBM heater control module, which also ensures the module's safety by automatically disabling the power supply should any of the heated wall temperatures exceed 125 °C (occurring only during the CHF transient for experiments using FC-72 as working fluid). Upon exiting the test section, the fluid passes through a Lytron air-cooled condenser to convert the fluid back to a subcooled, single-phase liquid state before it passes an accumulator and returns to the pump.

Important to note for the present flow loop is the presence of pressure transducers upstream and downstream of all key fluid components within the loop. This level of measurement is necessary to achieve the first key objective listed in the preceding section, determination of the contribution of fluid component selection on flow boiling dynamic behavior.

Data throughout the system are obtained with an NI SCXI-1000 data acquisition system controlled by a LabVIEW code. Pressure transducer data are sampled at 200 Hz, allowing high fidelity transient analysis of pressure signals.

Two-phase interfacial features are captured along the heated length of FBM using a high-speed camera. A pixel resolution of 2040×170 and a frame rate of 2000 frames per second (fps) are used to capture images spanning the total 114.6-mm heated length for tests run in all three orientations. Illumination is provided from the opposite side of the flow channel by blue LEDs, with light passing through a light shaping diffuser (LSD) to enhance illumination uniformity.

2.3. Operating conditions, operating procedure, and measurement uncertainty

Operating conditions spanning vertical upflow, vertical downflow, and horizontal flow orientations are as follows: FC-72 inlet pressure of $P_{in} = 97.1–231.3$ kPa, inlet temperature of $T_{in} = 23.2 – 79.6$ °C, mass velocity of $G = 176.5 – 2442.5$ kg/m² s, and inlet thermodynamic equilibrium quality of $x_{e,in} = -0.57 – 0.20$. It is important to note that negative inlet quality relates to inlet subcooling by the relationship

$$x_{e,in} = \frac{Pwr_{PH} - \dot{m} c_{p,f}(T_{FC,sat} - T_{PH,in})}{\dot{m} h_{fg}}, \tag{1}$$
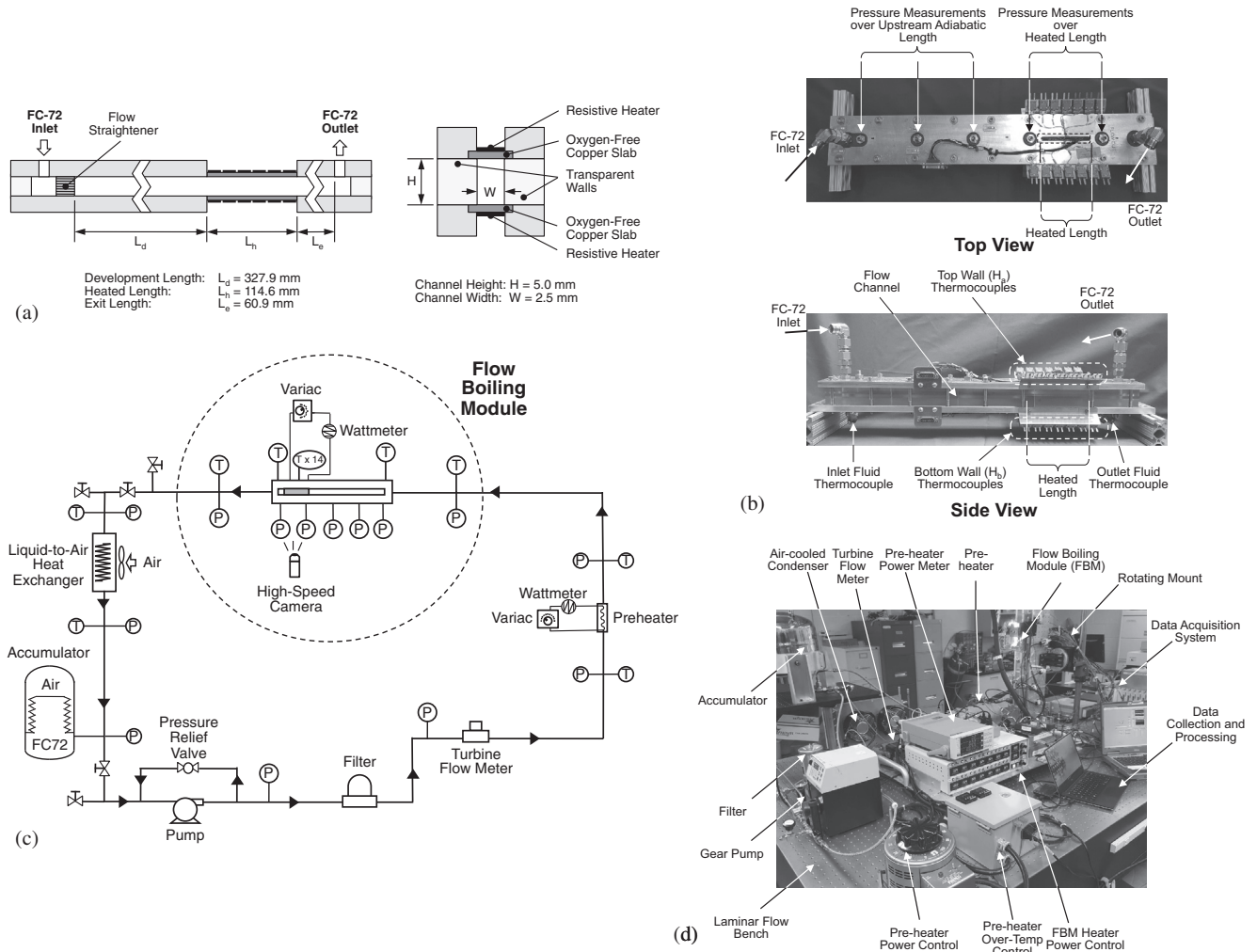
Fig. 1. (a) Flow boiling module (FBM) schematic. (b) Top and side views of FBM. (c) Flow loop schematic. (d) View of flow loop and key hardware within.

where Pwr_{PH} is the power supplied by the pre-heater, $\dot{m}$ is the mass flow rate, $T_{FC,sat}$ and $T_{PH,in}$ are saturation and inlet fluid temperatures at the preheater, respectively, and $c_{p,f}$ and h_{fg} are, respectively, the specific heat and latent heat of vaporization of the fluid. Negative inlet quality is used instead of subcooling to better represent the combined influence of transient pressure and mass velocity changes within the system.

Due to operational pressure constraints imposed by the FBM, operating conditions combining high inlet quality and high flow rate could not be achieved. Table 1 provides the combinations of mass velocity and inlet quality achieved for all three flow orientations.

Tests are initiated by setting pump speed and pre-heater power to achieve the desired inlet conditions. After monitoring temperature and pressure signals in the LabVIEW code to confirm steady state has been reached, power to the heated walls in the FBM is turned on, and heat flux is increased in small increments. After each increment, wall temperatures are monitored to determine when steady state is achieved, after which data are captured for an additional 30–60 s. In the present study, steady state is achieved when wall and fluid temperatures cease to change over a period of 15 s. Heated wall power is increased until CHF is encountered. Different from prior studies [31], however, is that the mass flow rate is no longer maintained by adjusting the pump as heat flux is increased. Instead, it is allowed to vary in response to changes in system pressure, information that is important for variable heat flux applications.

Type-E thermocouples with an accuracy of ±0.5 °C are used to measure fluid and heated wall temperatures throughout the facility. Pressure measurements throughout the flow loop are made

Table 1
Test matrix for study.

Mass velocity, G [kg/m² s]	Inlet condition			
	T_{sub} = −40 °C	$x_{e,in}$ = 0.00	$x_{e,in}$ = 0.10	$x_{e,in}$ = 0.20
~200	√	√	√	√
~400	√	√	√	√
~800	√	√	√	√
~1600	√	NA	NA	NA
~2400	√	NA	NA	NA

using pressure transducers with an accuracy of ±0.1%, which corresponds to an accuracy for all pressure drop measurements of ±0.2%. Pressure transducers used in the present study possess a mechanical response time of less than 1 ms, allowing the signal to be sampled at 200 Hz (once every 0.005 s). The turbine flow meter has an accuracy of ±0.1% and a mechanical response of 3–4 ms. The wall heat input is measured with an accuracy of ±0.5 W.

3. Analysis of system dynamics

3.1. Approach for determining influence of fluid components

As mentioned in the proceeding sections, pressure transducers are placed upstream and downstream of all key fluid components in order to isolate and characterize the contribution of individual components to overall system dynamic performance. As this resulted in an overly large amount of data, however, the current study will focus on five regions found to be of most interest within the system. These are depicted graphically in Fig. 2(a), with *Region I* corresponding to pressure drop across the filter, *Region II* pressure at the outlet of the pre-heater, *Region III* pressure drop across the heated length of the FBM (L_h in Fig. 1(a)), *Region IV* pressure drop across the condenser, and *Region V* pressure at the stream-wise location of the accumulator. These locations were selected based on the following rationale:

Region I: Pressure drop across the filter includes pressure information acquired at the outlet of the pump (which represents the primary mechanical component within the flow loop), while also providing representative information on the impact of the filter (an important fluid component) within the subcooled portion of the flow loop.

Region II: The outlet of the pre-heater represents the first location within the flow loop where, for test cases with saturated inlet conditions, two-phase flow pressure measurements are made within the loop. The pre-heater inlet was observed to exhibit dynamic behavior similar to that at the filter outlet, which is included in Region I.

Region III: Pressure drop across the heated length of the flow boiling module is the most critical measurement made in the present study. Improving upon prior work [31], using a larger number of fast response pressure transducers allows dynamic behavior within the test section in the present study to be compared with that at the outlet of the pre-heater to isolate the effect of boiling within the flow boiling module itself as opposed to behavior introduced by phase change within the pre-heater and propagated upstream.

Region IV: Pressure drop across the condenser is comprised of signals from both saturated (condenser inlet) and subcooled (condenser outlet) regions of the flow loop, allowing direct comparison of crucial phenomena in both regions for all operating conditions tested. Additionally, this pressure drop may reflect the influence of mechanical vibrations introduced by the condenser's fans.

Region V: The role of the accumulator within the flow loop is to accommodate volume changes introduced by phase change, and as such the height of bellows within the accumulator is expected to fluctuate in response to the system's dynamic behavior. Pressure measurement at the accumulator is expected to provide information on both overall loop dynamic behavior as well as the dynamics associated with response of the accumulator itself.

Adopting the approach successfully utilized in prior work [31], analysis will center on amplitude versus frequency plots generated

by performing fast Fourier transforms of transient pressure signals at locations of interest. Sample transient plots will also be presented for specified operating conditions in each region, however, as it is not only important to characterize flow oscillations by finding dominant frequencies and peak amplitudes, but also to understand how these oscillations manifest themselves in the time domain.

Fig. 2(b)–(e) provide plots of transient operating conditions for each of the key sets of inlet conditions investigated, depicted here with the test section in vertical upflow orientation. These plots are representative of the transient response of key operating conditions which will be used when comparing flow dynamic behavior at the aforementioned five regions of interest.

In each case, a near step function increase in heat flux applied to the FBM heated walls is followed by an increase in wall temperature asymptotically approaching a constant mean value while the instantaneous value continues to exhibit some fluctuation. The wall temperature used here is *T5* corresponding to the fifth thermocouple along the streamwise direction on the top wall for horizontal flow; relative location of this wall is inconsequential for vertical upflow and vertical downflow orientations. The temperature fluctuations are significantly larger for the cases with saturated inlet conditions, Fig. 2(c) and (e), than those with subcooled inlet conditions, Fig. 2(b) and (d). Similarly, both mass velocity and inlet quality exhibit significant fluctuations as they approach constant mean values, with higher amplitude fluctuations encountered in the cases with saturated inlet conditions. It is also worth noting that transient plots of inlet quality appear more 'dense' than those of mass velocity in each case, which can be attributed to mass velocity being a direct measurement, while quality is calculated according to Eq. (1) using several fluctuating parameters. More attention will be paid to the frequency composition of these signals in subsequent sections.

Mean values indicated in the plots were calculated by averaging over the final 30 s for each case. In addition to vertical upflow, subsequent figures will provide amplitude versus frequency plots for horizontal and vertical downflow orientations, both of which correspond to operating conditions similar to those for vertical upflow. The orientation of all measurement locations other than region III (test section) remains unchanged, but changes to test section orientation causes changes to manifest throughout the flow loop so it is reported for associated measurements at all regions of interest. Table 2 provides time-averaged operating conditions for each combination of test section orientation and inlet condition to be presented hereafter, with mass velocity, inlet quality, and inlet pressure all associated with the inlet to the heated length of FBM. Heat flux applied to the heated walls of FBM and critical heat flux (CHF) associated with the given inlet conditions are also provided.

3.2. Region I: Filter between pump and Pre-heater

Immediately upon exiting the pump, the fluid exhibits moderate pressure fluctuations. Fig. 3(a) depicts transient results for vertical upflow with G = 836.6 kg/m^2 s, which show that pressure drop across the filter oscillates within a 2–8 kPa envelope. The fact that the flow exhibits oscillations of similar amplitude both upstream and downstream of the filter is an important conclusion, implying that the filter itself plays little role in influencing system dynamic behavior.

Fig. 3(b)-(e) provide amplitude versus frequency plots of the same and show that oscillations are confined primarily to the high-frequency range (with noticeable frequency peaks in the 20–100 Hz range) of the plots. This is indicative of mechanically induced vibrations within the system, especially as the pump itself
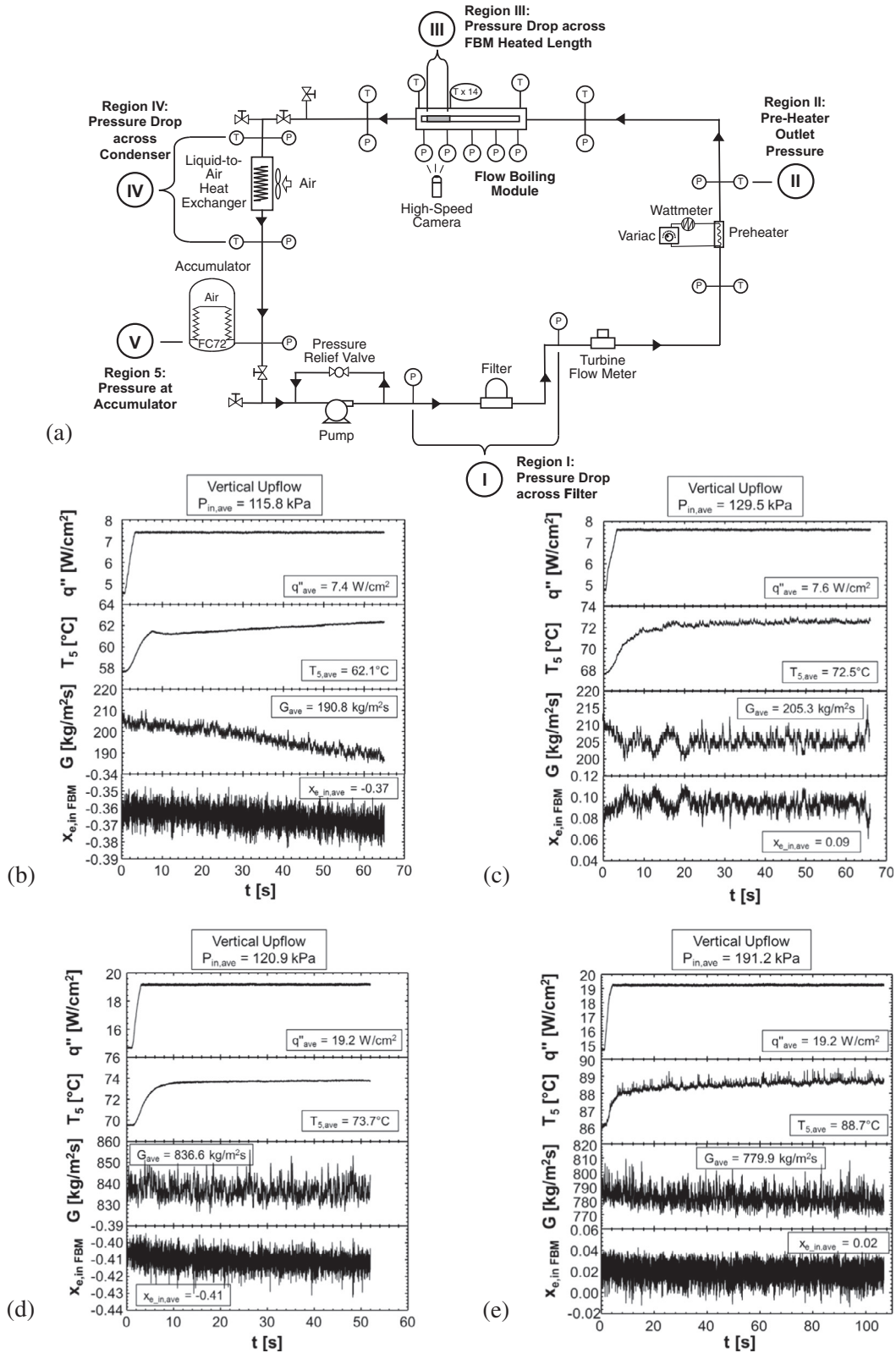
Fig. 2. (a) Five regions for analysis of dynamic pressure behavior, along with transient records of operating conditions for vertical upflow with (a) $G \sim 200$ kg/m^2 s and subcooled inlet, (b) $G \sim 200$ kg/m^2 s and saturated inlet, (c) $G \sim 800$ kg/m^2 s and subcooled inlet, and (d) $G \sim 800$ kg/m^2 s and saturated inlet.

is a prime source of vibrations resulting from its internal rotary motion.

Across Fig. 3(b)-(e) amplitudes vary greatly, with some cases (especially vertical upflow in Fig. 3(e)) exhibiting significantly

higher amplitude oscillations than other cases. Outliers aside, it is clear that Fig. 3(d) and (e) exhibit stronger dynamic behavior than Fig. 3(b) and (c). This trend can be attributed to the increase in mass velocity from $G \sim 200$ kg/m^2 s for Fig. 3(b) and (c) to

Table 2
Key operating conditions for system dynamic analysis cases. Indicated cases correspond to parts (b)–(e) in Figs. 2–8.

Case	Vertical upflow				
	G [kg/m^2 s]	$x_{e,in}$	$P_{FBM,in}$ [kPa]	q''_{FBM} [W/cm^2]	CHF [W/cm^2]
(b)	190.8	−0.37	115.8	7.4	22.5
(c)	205.3	0.09	129.5	7.6	19.1
(d)	836.6	−0.41	120.9	19.2	44.6
(e)	779.9	0.02	191.2	19.2	28.9
Case	Vertical downflow				
	G [kg/m^2 s]	$x_{e,in}$	$P_{FBM,in}$ [kPa]	q''_{FBM} [W/cm^2]	CHF [W/cm^2]
(b)	203.1	−0.45	127.8	8.0	11.7
(c)	217.6	0.06	106.9	7.4	12.9
(d)	831.7	−0.54	132.5	20.4	25.4
(e)	792.3	0.04	194.6	20.3	28.4
Case	Horizontal flow				
	G [kg/m^2 s]	$x_{e,in}$	$P_{FBM,in}$ [kPa]	q''_{FBM} [W/cm^2]	CHF [W/cm^2]
(b)	191.9	−0.52	98.5	7.8	10.7
(c)	214.7	0.08	123.8	6.9	7.8
(d)	845.0	−0.44	108.3	19.5	32.4
(e)	783.6	0.02	183.7	19.4	22.0

$G \sim 800$ kg/m^2 s for Fig. 3(d) and (e), which comes with an increase in pump work imparted on the fluid and associated increase in magnitude of pump-induced oscillations.

As the fluid continues through the flow loop, it next passes the turbine flow meter. The turbine flow meter used in the flow loop incurred the single largest pressure drop of any component within the loop but, across all sets of operating conditions, was shown to have a negligible impact on dynamic behavior and is therefore omitted from analysis.

3.3. Region II: Pre-heater outlet and FBM inlet

The next component of interest within the flow loop is the pre-heater. Because of miniscule impact of the turbine flow meter on dynamic behavior, frequency composition of the transient pressure signal at the pre-heater inlet is nearly identical to that at the filter outlet for all cases tested.

Fig. 4(a) clearly depicts, however, for vertical upflow with $G \sim 800$ kg/m^2 s, that the transient pressure signal at the pre-heater's exit exhibits drastic differences depending on whether the fluid exits the pre-heater in a subcooled or saturated state. While system pressure at the pre-heater's outlet is much higher for the saturated mixture case ($x_{e,in} = 0.02$), the magnitude of pressure oscillations is clearly smaller than for the subcooled case ($x_{e,in} = −0.41$).

Fig. 4(b)-(e) also show that the frequency composition is much different for subcooled versus saturated cases. In Fig. 4(b) and (d), corresponding to $G \sim 200$ kg/m^2 s and 800 kg/m^2 s, respectively, with subcooled inlet conditions, it is clear that much of the oscillatory behavior is confined to a range of 5–30 Hz, with some smaller peaks also present in the higher 80–100 Hz range. The only exception is the general upward trend of the plots in Fig. 4(b) with decreasing frequency below 1 Hz. This is likely due to the larger time constants associated with loop operation at low flow rates, which can drive gradual changes in system operating conditions that are not always immediately apparent while running experiments.

In Fig. 4(c) and (e), corresponding to saturated inlet conditions, peak frequencies of oscillation are found in the 0.1–1 Hz range, and little to no oscillations are seen above 15 Hz. The only exception is the case of vertical downflow in Fig. 4(c), which, despite boiling taking place within the pre-heater, continues to exhibit dominant oscillatory modes in the high frequency range similar to those expected for subcooled conditions. It is possible that this behavior is related to the relatively large vertical distance the fluid must travel to reach the inlet of the test section for tests performed in this orientation. In the vertical downflow cases with $G = 217.6$ kg/m^2 s, low flow inertia allows body force to play a more dominant role, and distribution of bulk flow between liquid and vapor phases becomes less predictable. This potentially provides a continuous liquid path for high-frequency oscillations to propagate not present in the other flow orientations.

Also of note in Fig. 4(c) and (e) is the presence of dominant frequencies in the 0.1–5 Hz range. As noted in prior work [31], this behavior is consistent with density wave oscillations, and will be analyzed in greater detail in conjunction with the FBM response.

3.4. Region III: Flow boiling module (FBM)

Fig. 5(a) illustrates, for vertical upflow, the significant difference in amplitude of pressure drop oscillations across the heated length of the FBM between cases with subcooled inlet conditions and those with saturated inlet conditions. This runs counter to the trend seen in Fig. 4(a), where boiling within the pre-heater was seen to have a stabilizing effect on fluid dynamic behavior. The opposing trends for the FBM and pre-heater can be explained by examining the internal geometry of each: the pre-heater consists of a 12.7-mm i.d. tube coiled multiple times around three cartridge heaters for a total length of 3810 mm, all mounted within a large assembly, while the heated portion of the FBM (described in Section 2) possesses a hydraulic diameter of 3.33 mm and a much shorter 114.6-mm heated length. These differences in geometry mean that, even though more power is supplied by the pre-heater, the heat flux applied to the much larger heated area within the pre-heater is lower than that applied to the smaller heated walls within the FBM. In the present study, the highest heat flux achieved within the FBM was 50.8 W/cm^2, while heat flux within the pre-heater never exceeded 0.6 W/cm^2. The higher heat fluxes applied to the FBM yield more vigorous phase change within the test section, leading to more dynamic flow behavior.

Like Fig. 4(b)-(e), there are appreciable differences in frequency composition of transient pressure signals for subcooled versus saturated inlet conditions. Fig. 5(b) and (d), corresponding to subcooled inlet conditions with $G \sim 200$ kg/m^2 s and 800 kg/m^2 s, respectively, again exhibit dominant frequencies in the high frequency range, although amplitudes of oscillation are now much
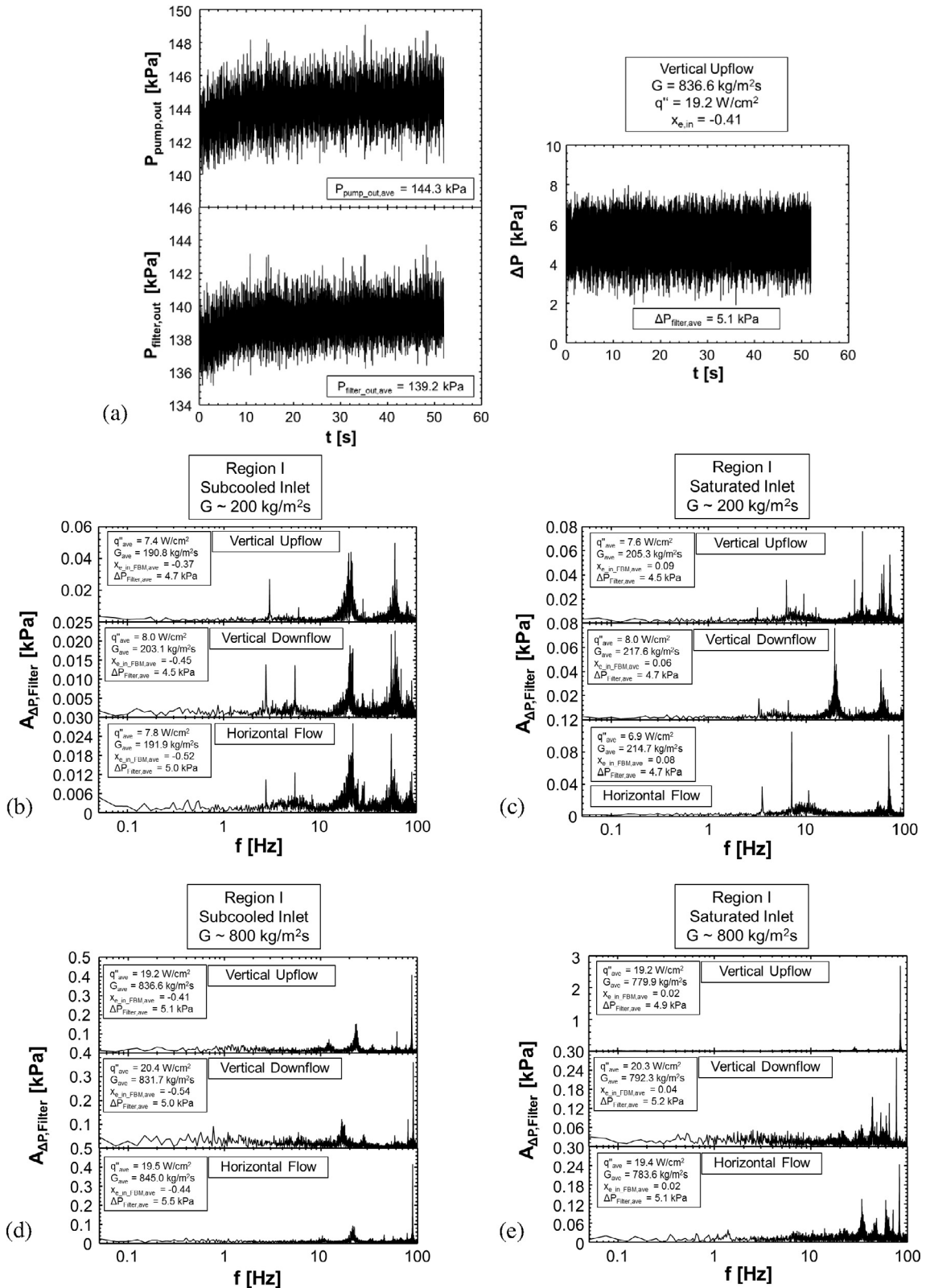
Fig. 3. (a) Sample plot of transient pressure drop across the filter (region 1), along with amplitude versus frequency plots of the same for vertical upflow, vertical downflow, and horizontal flow with (b) $G \sim 200$ kg/m^2 s and subcooled inlet, (c) $G \sim 200$ kg/m^2 s and saturated inlet, (d) $G \sim 800$ kg/m^2 s and subcooled inlet, and (e) $G \sim 800$ kg/m^2 s and saturated inlet.

lower and feature fewer sharp peaks. This reduction in amplitude and the 'smearing' across the frequency spectrum of upstream well-defined, mechanically induced oscillatory modes is attributed

to subcooled boiling along the heated walls within the test section followed by the rapid 'collapse' of bubbles back to single-phase liquid as they detach from the wall and enter the bulk, subcooled
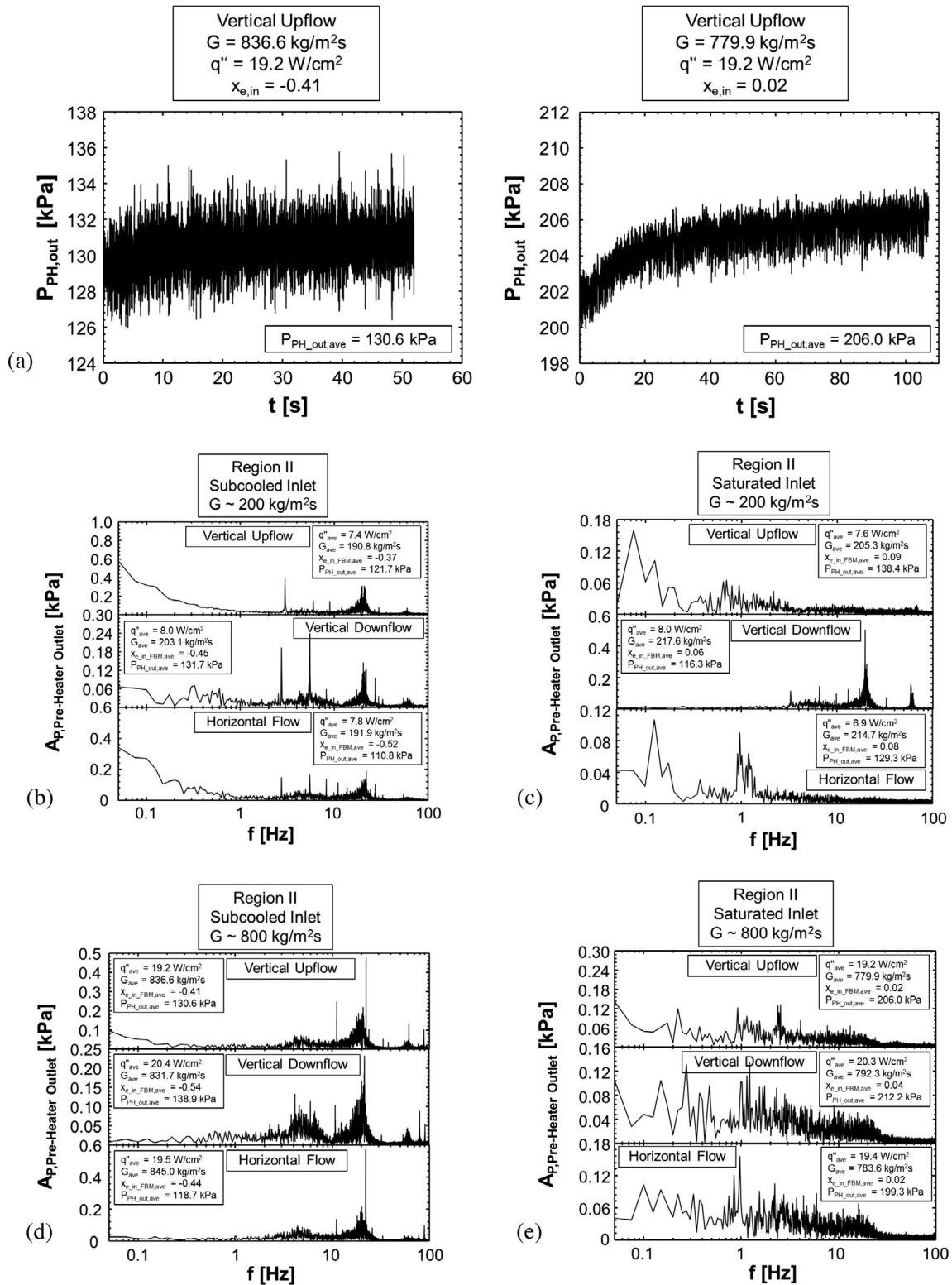
Fig. 4. (a) Sample plot of transient pre-heater outlet pressure (region II), along with amplitude versus frequency plots of the same for vertical upflow, vertical downflow, and horizontal flow with (a) $G \sim 200$ kg/m^2 s and subcooled inlet, (b) $G \sim 200$ kg/m^2 s and $x_{e,in} \sim 0.10$, (c) $G \sim 800$ kg/m^2 s and subcooled inlet, and (d) $G \sim 800$ kg/m^2 s and $x_{e,in} \sim 0.05$.

flow. It should be noted that negative values of time-averaged pressure drop shown for the vertical downflow and horizontal flow orientations with subcooled inlet conditions, Fig. 5(b) and (d), are attributed to difficulties in measuring very small pressure drops coupled with limitations in measurement accuracy of the pressure transducers used.

Fig. 5(c) and (e), which correspond to saturated inlet conditions with $G \sim 200$ kg/m^2 s and 800 kg/m^2 s, respectively, exhibit peak frequencies of oscillation in the range of 0.1–5 Hz, similar to those seen in Fig. 4(c) and (e), with the case of vertical downflow with G = 217.6 kg/m^2 s again proving to an exception, likely for the afore-mentioned reasons. This behavior is consistent with that attributed
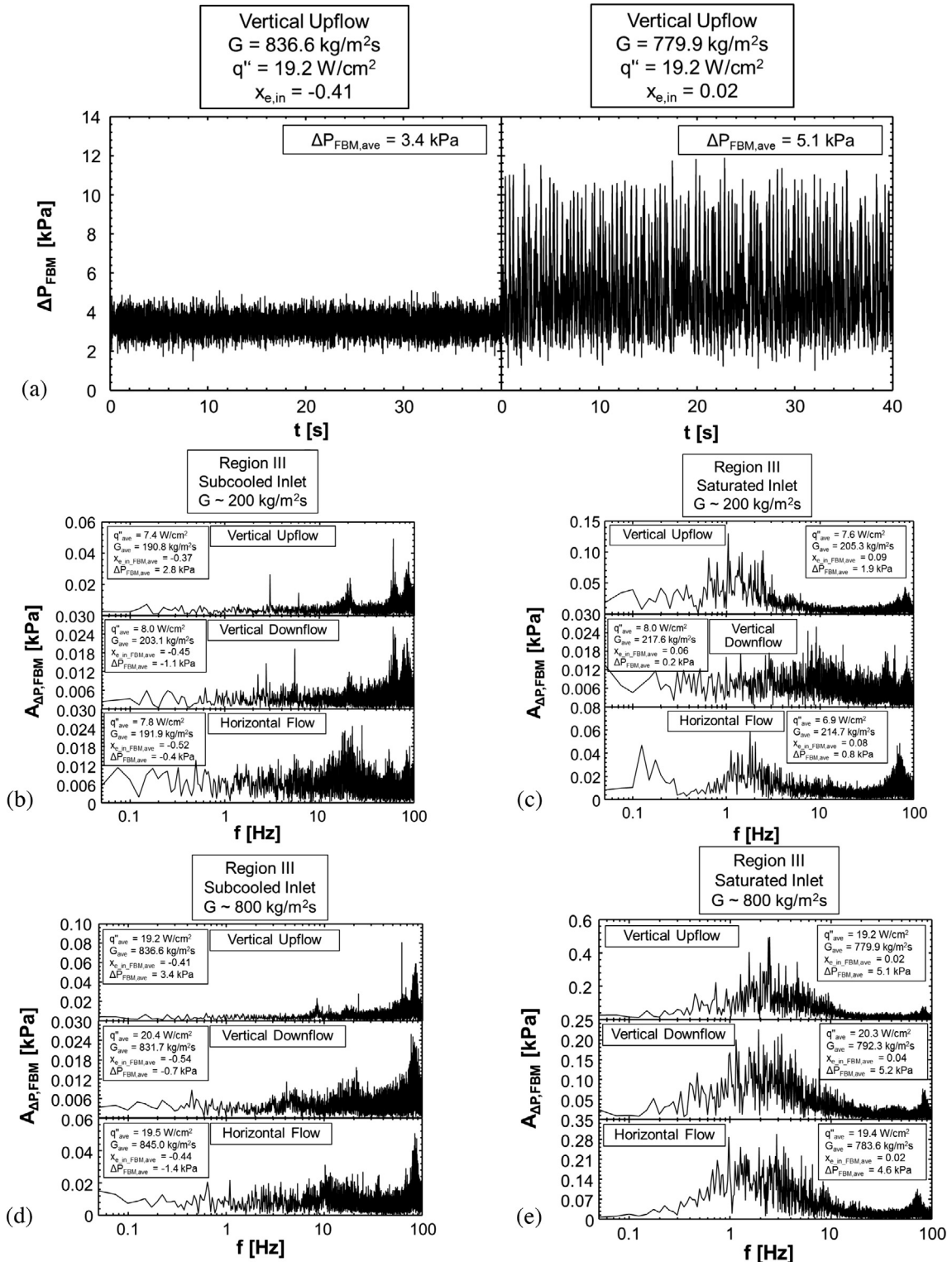
Fig. 5. (a) Sample plots of transient pressure drop across heated length of FBM (region III), along with amplitude versus frequency plots of the same for vertical upflow, vertical downflow, and horizontal flow with (a) $G \sim 200$ kg/m^2 s and subcooled inlet, (b) $G \sim 200$ kg/m^2 s and saturated inlet, (c) $G \sim 800$ kg/m^2 s and subcooled inlet, and (d) $G \sim 800$ kg/m^2 s and saturated inlet. Negative values of average pressure drop reported for highly subcooled inlet conditions in vertical downflow and horizontal flow orientations are attributed to difficulties in measuring small pressure drops coupled with limitations in measurement accuracy.

to Density Wave Oscillations (DWOs) by Boure et al. [28], but more thorough investigation is warranted to establish that these low frequency pressure oscillations are indeed due to DWOs.

Fig. 6(a)–(c) provide a clear depiction of the phenomenon described herein as Density Wave Oscillations (DWOs). Fig. 6(a)

presents flow visualization images taken of the heated length of FBM with inlet conditions corresponding to those of Fig. 5(e) with vertical upflow orientation. It is difficult to distinguish specific flow features because of finite quality at the inlet to the test section, but it is very clear that at different times the region of interest is

alternatively composed of predominantly vapor (images are bright due to high transmission of light) and predominantly liquid (images are dark due to low transmission of light). In particular, there are short time windows where the heated length of FBM is almost entirely occupied by liquid, which are always followed by a period in which liquid content decreases and vapor increases, only for another large liquid region to pass through shortly after.

It is this cyclical passage of High Density Fronts (HDFs) followed by periods of high vapor void fraction (Low Density Fronts) that is termed Density Wave Oscillations in the present study. Fig. 6(b) helps illustrate this by tabulating the times associated with successive passage of HDFs. By calculating the difference in time between HDFs, single-event frequencies can be calculated ($f = 1/\Delta t$), which are seen to fall perfectly within the frequency range of dominant pressure oscillations depicted in Fig. 6(c) (which is taken directly from Fig. 5(e)). It should be noted here that time $t = 0$ s is associated with the onset of image acquisition and has no physical meaning.

On the analytic side, the attribution of these low-frequency pressure fluctuations to DWOs is further reinforced by the work of Lahey and Podowski [54], who stated that resonant frequency f_r of a system experiencing DWOs can be expressed as

$$f_r = \frac{1}{2T_{tr}} \sim \frac{U_{FC-72}}{2L_{ts}}, \tag{2}$$

where T_{tr} is the transport time, U_{FC-72} the velocity of the working fluid, and L_{ts} the heated length of the test section. In general terms, this equation indicates that the frequency is equal to the inverse of twice the residence time of the disturbance on the heated wall. Here, disturbance propagation speed is approximated by liquid velocity assuming the flow is made of liquid alone. Evaluating this relationship for the conditions represented in Fig. 5(c) and (e) and comparing with experimentally observed dominant frequencies of oscillation yield the values given in Table 3. This table shows relatively good agreement for higher mass velocities but significant error for lower mass velocities. Additionally, even for higher mass

HDF Occurrence	Time [s]	Δt [s]	f [Hz]
1	0.3	-	-
2	0.5625	0.2625	3.81
3	1.0375	0.475	2.11
4	1.225	0.1875	5.33
5	1.825	0.6	1.67
6	2.225	0.4	2.5

(b)
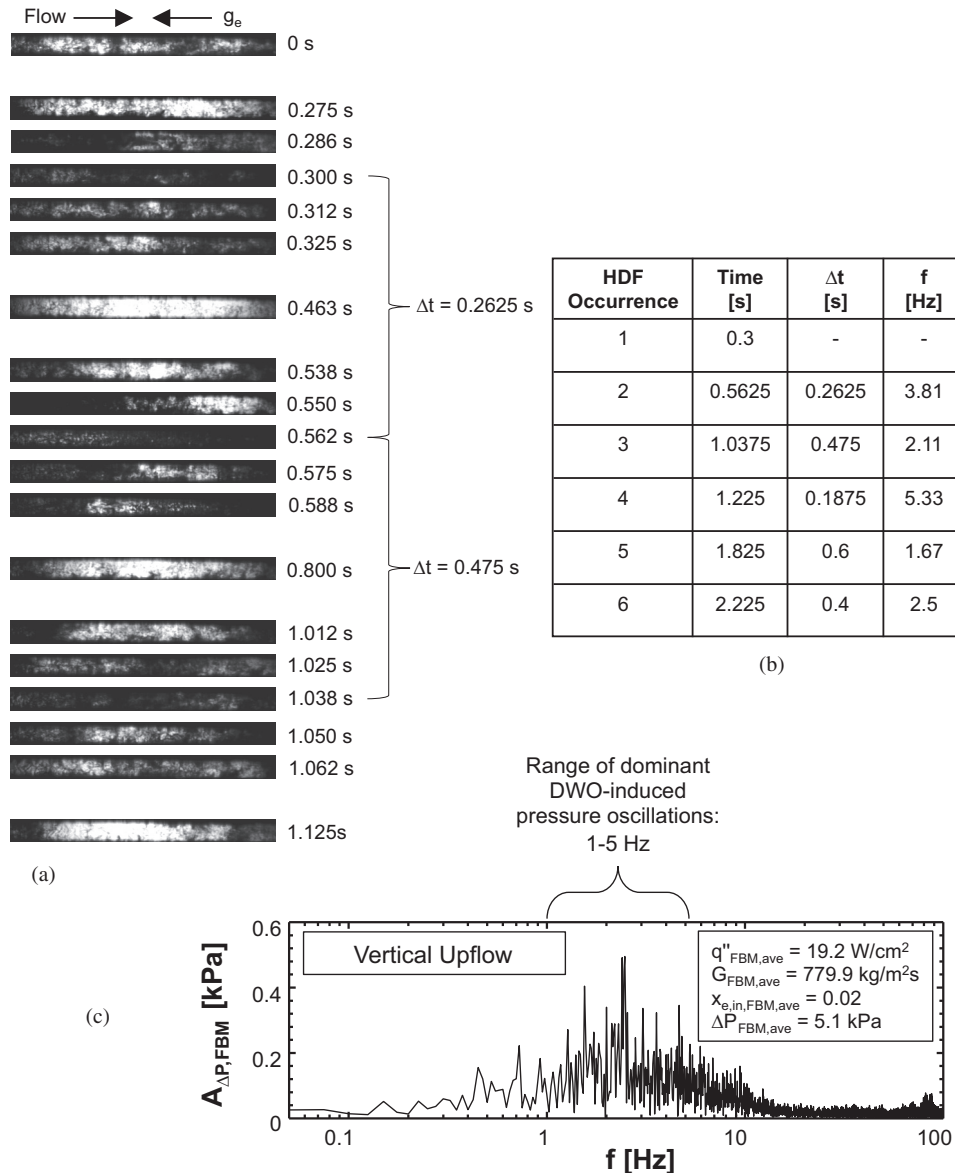
Fig. 6. (a) Flow visualization images depicting the cycle of low density (bright) and high density (dark) fronts passing through the heated length of FBM in vertical upflow with finite inlet quality, with (b) six consecutive High Density Fronts (HDFs) identified from images and the time between them used to calculate single-event frequencies, which are shown to fall within the range of peak oscillatory behavior in (c).

velocities, the frequency prediction remains static while differences are seen in experimental results for the three orientations. Both trends indicate the inability of Eq. (2) to account for body force effects. This error might be related to the inaccuracy of approximating disturbance speed with bulk liquid velocity, and might be corrected by implementing more sophisticated modeling for disturbance propagation speed.

3.5. Region IV: Condenser

Exiting the FBM, the fluid travels to the condenser, where it is converted back to single-phase liquid. Fig. 7(a) shows transient pressure signals for both the condenser inlet and outlet, illustrating clear differences between the two for the case of saturated flow boiling within the FBM. The pressure at the condenser inlet appears very similar to that at the FBM outlet for saturated flow boiling cases, while the pressure at the condenser outlet resembles that downstream of the pump for all cases. This reinforces the idea introduced in conjunction with Fig. 4, that pressure oscillations in single-phase liquid regions are dominated by high frequency, mechanically induced phenomena, while fluctuations in the two-phase (saturated) regions exhibit negligible influence from mechanical factors and are instead dominated by physical two-phase phenomena, such as DWOs.

Fig. 7(b)-(e) reinforce this idea by revealing that pressure oscillations across the condenser are dominated by the sharp, high frequency peaks associated with mechanically induced oscillations. It is unclear whether these oscillations are propagated upstream from the pump (as the flow is subsonic in all cases), or induced by vibrations from the two condenser air fans. Fig. 7(e), however, illustrates that, for high mass velocity saturated flow boiling cases, DWOs at the inlet become non-negligible when analyzing transient pressure drop results. It is possible that at even higher mass velocities the increased amplitude of DWOs will render them the dominant factor in transient pressure drop fluctuations across the condenser.

3.6. Region V: Accumulator

After returning to single-phase liquid in the condenser, the fluid makes its way past the accumulator. Fig. 8(a) shows drastic differences in the pressure measured at the accumulator even for similar operating conditions, with the same flow rate yielding negligible (~1 kPa) pressure fluctuations in the case of subcooled boiling upstream, while more appreciable pressure fluctuations (~8 kPa) are seen for the case of saturated boiling upstream. Fig. 8(b)-(e) prove that consistent trends regarding upstream conditions or test section orientation cannot be drawn, with both amplitude and frequency of dominant oscillations varying widely across the parametric ranges evaluated.

The only consistent trend seen across Fig. 8(b)-(e) is the damping of oscillations in the moderate (0.5–10 Hz) range, with oscillations observed only in the high (10–100 Hz) and low (<0.5 Hz) ranges. This could be due to the internal dynamics of the accumu-lator itself, as its design necessarily incorporates a mass-spring-damper system with its own mechanical bandwidth.

3.7. Overall outcomes

By analyzing pressure oscillations using high-frequency pressure measurements upstream and downstream of all major fluid components of the flow loop, two key conclusions are drawn which will be of use in subsequent analysis:

(1) Pressure oscillations within all portions of the flow loop occupied by single-phase liquid are dominated by high frequency mechanically induced phenomena. This includes subcooled flow boiling within the test section, although the process of bubble nucleation, departure, and collapse eliminates the sharp peaks seen elsewhere and distributes oscillations across the high frequency range.
(2) In cases where saturated flow is introduced by the pre-heater, pressure fluctuations are dominated by behavior characteristic of Density Wave Oscillations (DWOs). Additionally, high frequency pressure oscillations present in the upstream single-phase liquid portion of the flow loop are not present in the portion containing a two-phase mixture, but reappear downstream of the condenser once the fluid has been returned to single-phase liquid.

The second outcome is of particular importance as it allows analysis of dynamic behavior within the two-phase portion of the test loop to focus on physical explanations without fear of mechanically induced phenomena compromising the integrity of results.

4. Analysis of flow boiling transient behavior

4.1. Recap of trends from prior investigation

Previous work by the present authors [31] included analysis of parametric trends relating to magnitude of DWOs manifest in transient pressure drop across the heated length of FBM in flows with saturated inlet conditions. Key trends are presented in Fig. 9, as the same analysis will not be repeated in the present work, but rather expanded to include the effects of DWOs on other key parameters. It should be noted that the prior study did not address subcooled inlet conditions or dynamic response of regions other than the FBM.

Fig. 9(a) illustrates that, as mass velocity is increased, the amplitude of pressure oscillations also increases. This trend was observed again in the proceeding section in conjunction with saturated boiling conditions in Figs. 5 and 7. It should also be noted that there are threshold mass velocities required for DWOs to manifest themselves, which were encountered in the previous study for horizontal flow and vertical downflow orientations, but not for vertical upflow. In the present study this was seen only with vertical

Table 3
Predicted and experimental frequencies for DWOs shown in Fig. 5(c) and (e).

Orientation	G [kg/m² s]	$x_{e,in}$	$f_{DWO,pred}$ [Hz]	$f_{DWO,exp}$ [Hz]	Error [%]
Vertical Upflow	205.3	0.09	0.57	1.10	48.2%
Vertical Downflow	217.6	0.06	0.57	Unclear	–
Horizontal Flow	214.7	0.08	0.57	1.80	68.3%
Vertical Upflow	787.5	0.02	2.18	2.48	13.8%
Vertical Downflow	792.3	0.04	2.23	1.93	13.5%
Horizontal Flow	783.6	0.02	2.18	0.98 (2.90)[a]	55.0% (33.0%)[a]

[a] Different values for horizontal flow at the higher mass velocity correspond to two different peaks of nearly identical amplitude.
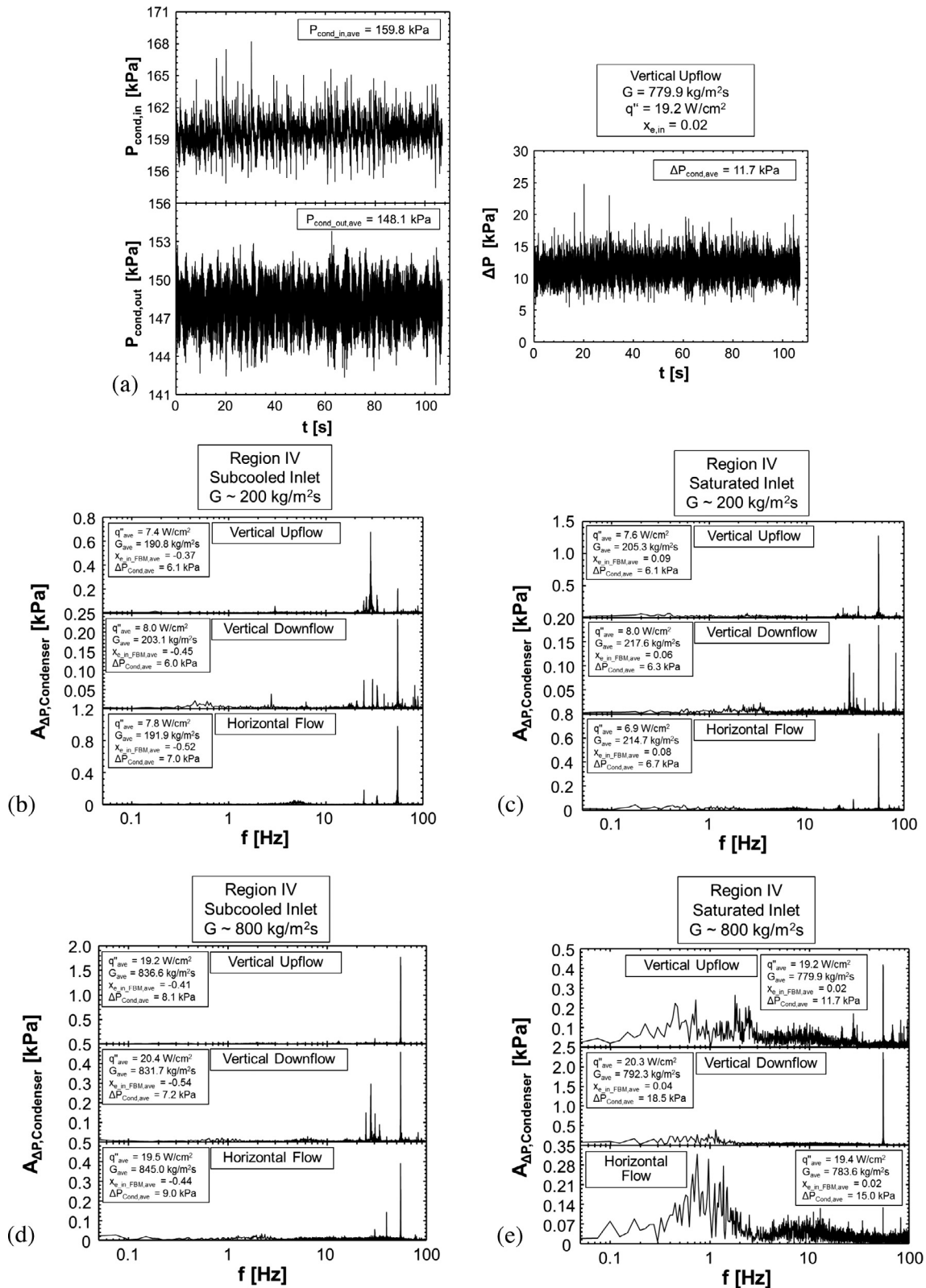
Fig. 7. (a) Sample plot of transient pressure drop through the condenser (region IV), along with amplitude versus frequency plots of the same for vertical upflow, vertical downflow, and horizontal flow with (a) $G \sim 200$ kg/m^2 s and subcooled inlet, (b) $G \sim 200$ kg/m^2 s and saturated inlet, (c) $G \sim 800$ kg/m^2 s and subcooled inlet, and (d) $G \sim 800$ kg/m^2 s and saturated inlet.
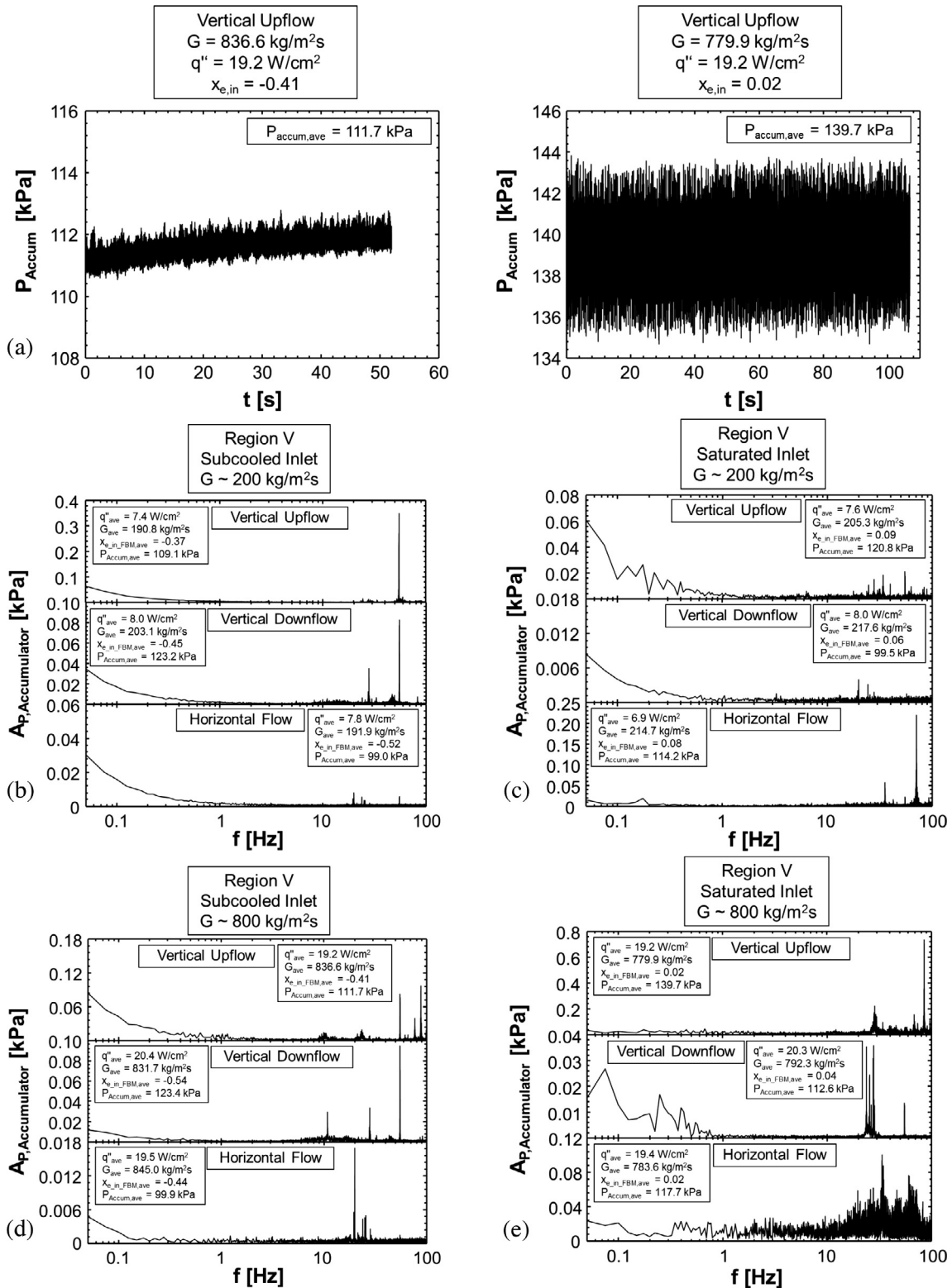
Fig. 8. (a) Sample plot of accumulator transient pressure (region V), along with amplitude versus frequency plots of the same for vertical upflow, vertical downflow, and horizontal flow with (a) $G \sim 200$ kg/m^2 s and subcooled inlet, (b) $G \sim 200$ kg/m^2 s and saturated inlet, (c) $G \sim 800$ kg/m^2 s and subcooled inlet, and (d) $G \sim 800$ kg/m^2 s and saturated inlet.

downflow, Fig. 5(c). This is likely due to differences in height of the test section for the two studies.

Similarly, Fig. 9(b) shows flow dynamic behavior increases as the heat flux is increased. This makes intuitive sense, as more vigorous boiling increases dynamic behavior within the test section.

Finally, Fig. 9(c) depicts the inconsistent impact of increasing quality on amplitude of pressure fluctuations. Tests conducted in vertical upflow orientation saw increased pressure fluctuations as inlet quality was increased, while horizontal flow experienced noticeable decreases in fluctuations. Tests performed in vertical
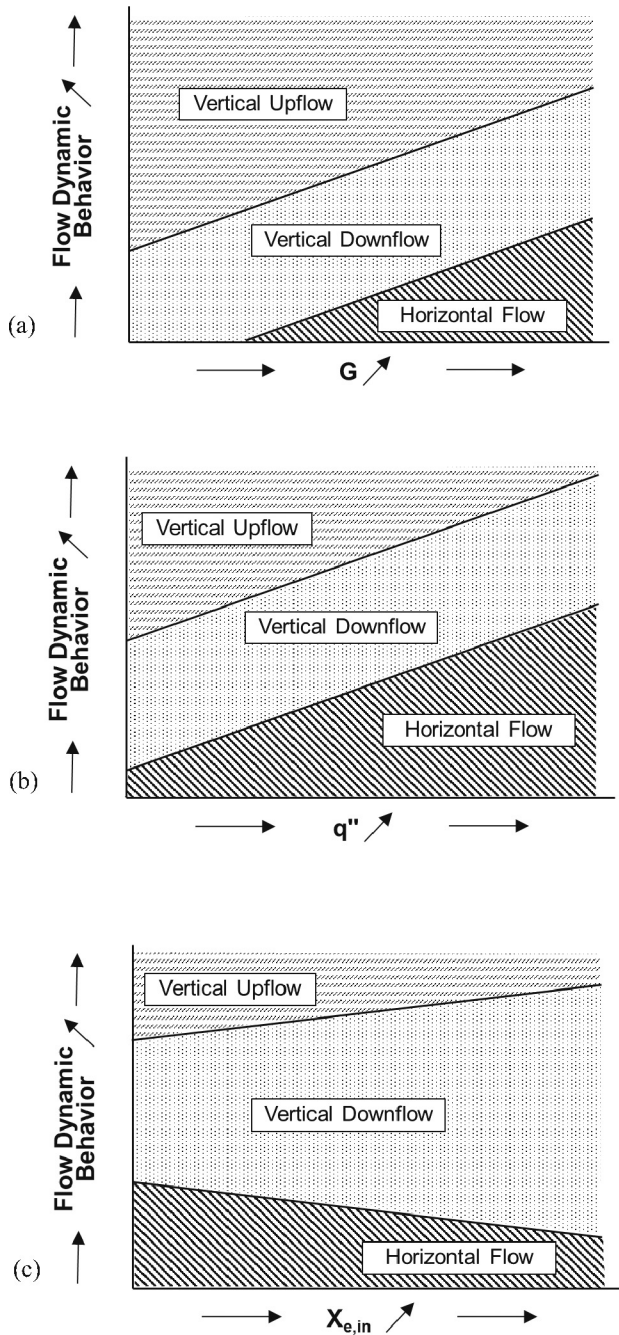
Fig. 9. Qualitative trends for magnitude of flow boiling dynamic behavior in FBM versus (a) mass velocity, (b) heat flux, and (c) inlet quality.

downflow orientation were largely unaffected by changes in inlet quality.

4.2. Transient evolution of key parameters with increases in heat flux

As outlined in Section 2, tests in the present study were run by using the pump and pre-heater to set a desired flow rate and thermodynamic state at the inlet of the test section prior to applying heat flux to the test section. Heat flux on the heated walls of the FBM was increased in discrete steps, with step size decreasing as CHF was approached, until CHF was achieved and the power supply deactivated to prevent damage to the test section. During this process, no changes were made to pump speed or pre-heater

power, allowing system pressure, flowrate, and inlet quality to evolve naturally in response to the boiling taking place along the heated length of the FBM.

Fig. 10(a) shows the applied heat flux steps, along with the evolution of heated wall temperature, pressure drop over the heated length of the FBM, test section mass velocity, and inlet quality over time for the case of subcooled flow boiling with $G \sim 400$ kg/m^2 s in vertical upflow orientation. The key feature of this plot is the change in amplitude of pressure drop oscillations between 400 and 600 s along with accompanying decreases in mass velocity and inlet quality. This is due to a transition from *bubbly flow* to *churn flow* as boiling intensity is increased within the test section, clearly seen in associated high speed images. It should also be noted that, as CHF is encountered (just before 1000 s) and power supplied to the heated walls drops to zero, the magnitude of pressure drop oscillations rapidly diminishes, and both mass velocity and inlet quality climb steeply towards their zero heat flux values, clearly demonstrating the strong influence of heat flux on transient flow behavior.

Fig. 10(b) shows similar plots for vertical upflow with $G \sim 400$ kg/m^2 s, this time with saturated inlet conditions instead of subcooled. Counter to the case of subcooled flow boiling, which exhibited a clear transition region in the range of 400–600 s, saturated flow boiling shows a largely linear change in both amplitude of pressure oscillations and system mass velocity as heat flux is increased within the test section. Inlet quality, while possessing large oscillations in the range of $x_{e,in}$ = 0.02–0.06, shows a generally neutral trend as heat flux within the test section is increased and mass velocity decreases. Similar to Fig. 10(a), parameter values quickly return to their zero heat flux values after CHF is encountered and heat flux returned to zero.

Fig. 10(c) shows a comparison of amplitude versus frequency plots of each parameter of interest for the lowest non-zero heat flux - heat flux 'C' from Fig. 10(a) and (b). Similar to Figs. 3–8, mean values indicated in Fig. 10(c) are calculated by averaging over the final 30 s of this heat flux. Immediately apparent is that the oscillations of heat flux are of such low magnitude as to have negligible impact on system dynamics. Temperature fluctuations are confined primarily to the low end of the frequency spectrum, which makes intuitive sense, as the thermal mass of the copper slabs used to create heated walls within the test section acts as a low-pass filter for thermocouple measurements performed within the walls.

It is in the amplitude versus frequency plot of pressure drop across the heated length of the test section where interesting behavior begins to emerge. For the subcooled inlet case, pressure fluctuations are dominated by a high frequency, well defined peak, similar to behavior seen for subcooled inlet cases examined previously in Fig. 5(b) and (d). Pressure fluctuations for the saturated inlet case exhibit behavior consistent with DWOs, with a peak frequency of ~2 Hz, and no appreciable oscillations in the high frequency range.

Similar differences can be seen in amplitude versus frequency plots of mass velocity, with oscillations in the subcooled inlet case dominated by a single, sharp peak around 6 Hz, while fluctuations for the saturated inlet are dominated by higher-amplitude peaks distributed across the 0.5–2 Hz range. This is due to the influence of DWOs manifest in system mass velocity, which is also seen in the plot for inlet quality fluctuations for saturated inlet conditions. It is very clear that for both saturated and subcooled inlet conditions, frequency composition of inlet quality fluctuations is nearly identical to that for mass velocity fluctuations. This is due to the direct presence of mass flowrate in Eq. (1), while pressure fluctuations are only indirectly present in the evaluation of saturation properties.

Finally, Fig. 10(d) shows amplitude versus frequency plots for the highest heat flux tested prior to CHF - heat flux 'D' from
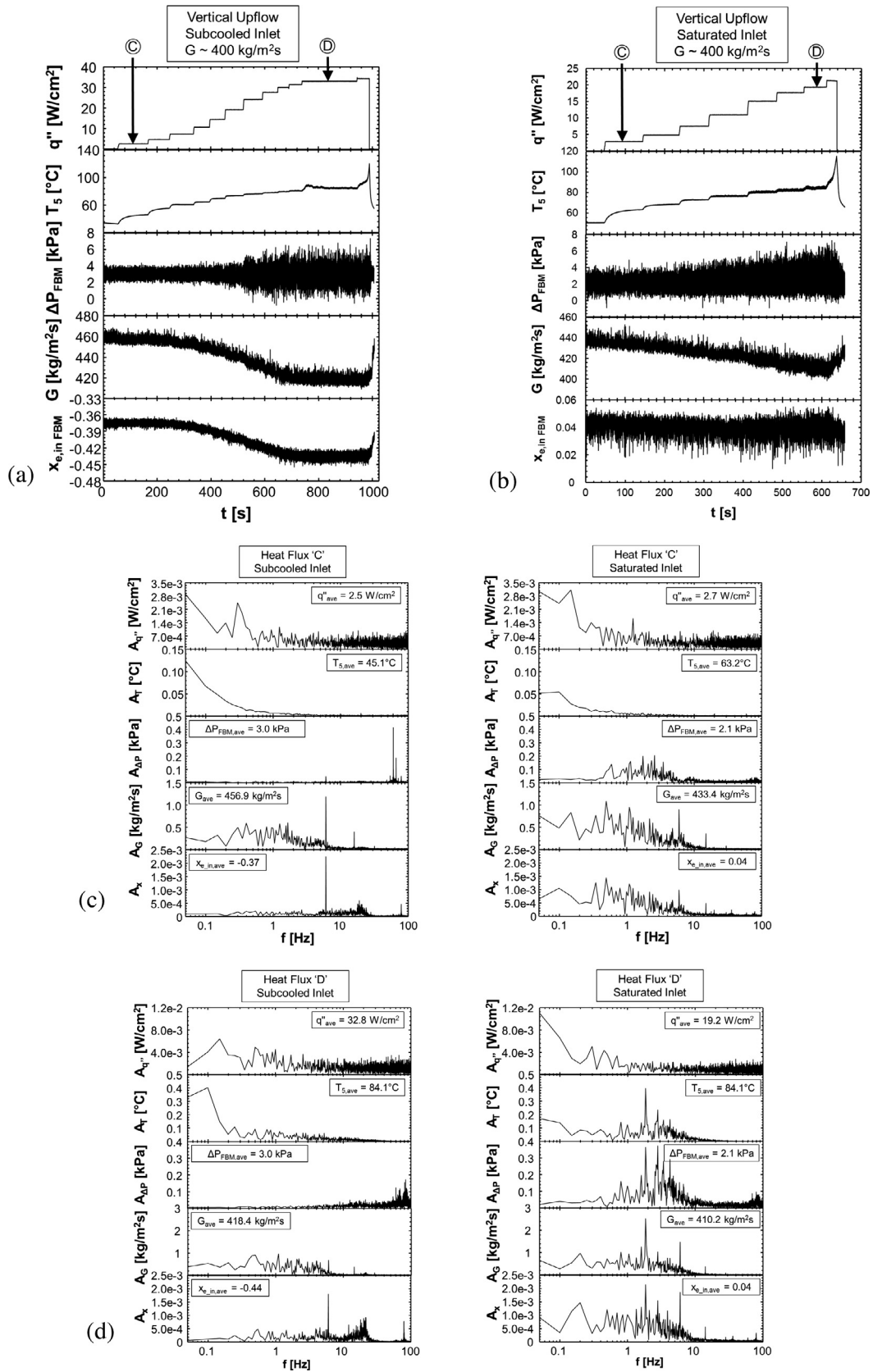
Fig. 10. Transient results for vertical upflow with (a) highly subcooled and (b) saturated inlet conditions. Fast Fourier transforms of key steady-state parameters corresponding to heat fluxes levels 'C' and 'D' for each are compared in (c) and (d).

Fig. 10(a) and (b). Results for the saturated inlet case show behavior attributable to DWOs again clearly dominates results for pressure drop, mass velocity, and inlet quality fluctuations, but now also significantly impacts heated wall temperature fluctuations. This is in itself an important observation as, depending on the amplitude of temperature oscillations, the possibility exists that CHF can be encountered due to heated wall temperature fluctuations exceeding a threshold value.

Parameters shown for the subcooled inlet case in Fig. 10(d) exhibit frequency composition similar to their low heat flux counterparts in Fig. 10(c), with the exception of subcooled boiling pressure drop fluctuations, which show significant 'smearing' of peaks across the high frequency range. As described when analyzing Fig. 5(b) and (d), this behavior is due to vigorous boiling along the heated walls, followed by bubble departure from the wall and bubble collapse after entering the bulk, subcooled flow.

Fig. 11(a)-(d) show results for similar operating conditions, now tested in vertical downflow orientation. Immediately apparent is the lack of a well defined transition region in Fig. 11(a) similar to that seen in Fig. 10(a). This can be attributed to the role of body force acting to stabilize liquid flow in the vertical downflow configuration, while it was destabilizing for vertical upflow. Fig. 11(b) shows, however, that there is a well defined transition point at ~400 s for the saturated inlet case, past which the magnitude of pressure drop fluctuations increases significantly and mass velocity drops sharply. This can be attributed to vapor production within the test section reaching a level where buoyancy force attempting to drive vapor counter to the flow direction begins to have a significant destabilizing effect on the flow. This effect is not seen for the subcooled case in Fig. 11(a), as (i) overall flow quality is much lower, and (ii) some vapor produced at the wall condenses back to liquid due to the bulk subcooling present.

Fig. 11(c), comparing amplitude versus frequency plots for subcooled and saturated inlet cases with low heat flux, exhibits results very similar to those seen for vertical upflow in Fig. 10(c), with DWO behavior dominating for the saturated inlet case and higher frequency modes present in the subcooled inlet case.

Similarly, Fig. 11(d) reinforces conclusions drawn when analyzing Fig. 10(d), namely the presence of significant DWO induced behavior for all parameters (except heat flux) in the saturated inlet case. The presence of large amplitude temperature oscillations for the higher heat flux, saturated inlet case is again particularly worth noting for its potential to initiate CHF. Unlike Fig. 10(d), however, DWO induced oscillations in Fig. 11(d) show a dominant frequency of ~1 Hz. This clear change in frequency with orientation reinforces the need for more sophisticated modeling to predict disturbance transport speed in Eq. (2).

Fig. 12(a)-(d) provide similar information for the case of horizontal flow. Immediately noticeable in Fig. 12(a) is a clear decrease in pressure drop across the heated length associated with the onset of boiling in the test section, followed by a gradual increase as boiling intensity is increased towards CHF. Mass velocity and inlet quality, however, exhibit only a gradual change in this same region, and do not begin to decrease significantly until heat fluxes close to CHF are applied.

Fig. 12(b) exhibits higher amplitude oscillations for pressure, mass velocity, and inlet quality than those seen in Fig. 12(a), but both are relatively stable compared to their counterparts seen in Figs. 10 and 11 for vertical upflow and vertical downflow, respectively. This indicates that, within the boiling region of the test section, stability is strongly influenced by the component of body force acting parallel or opposite to flow direction. This notion is reinforced in Fig. 12(c) and (d), which show that, while similar trends regarding the appearance and impact of DWOs seen for vertical upflow and downflow are present in horizontal flow, amplitudes of oscillation are greatly reduced.

5. Stability map evaluation

5.1. Utilization of stability maps in two-phase flow analysis

Maps for flow boiling stability have been available in the literature for many decades, but little work has been done to homogenize and evaluate them compared to that done for other simple design tools such as flow regime maps and predictive correlations. In fact, significant variations exist among different maps in terms of coordinates used to evaluate stability and even definition of stability. Some studies were concerned with mathematical instability of governing differential equations, while others demarcated 'stable' and 'unstable' zones of operation in relation to a single type of instability observed within the system in question. Table 4 presents information on five prior studies in which stability maps were presented, including working fluid, mass velocity and heat flux ranges, and operating geometry for those empiric in nature, as well as a definition of the concept of 'stability' or 'instability' used in each case. Also listed is similar information for the present study.

Fig. 13(a) and (b) depict stability maps originally presented by Bogojevic et al. [59] and Brutin and Tadrist [57], respectively, with stability boundaries indicated by dashed lines, and data from the present study superimposed over data used in the original studies. Notice that all present data in Fig. 13(a) are for vertical upflow orientation with subcooled inlet conditions for which DWOs were not observed. Although all the present data appear to correctly fall into the stable region of the map, it should be noted that this map was designed for a micro-channel heat sink and using water as working fluid. Additionally, the combinations of q'' and G corresponding to the unstable regions of the map could not be achieved in the present FBM. More importantly, use of dimensional parameters for the map axes precludes generalizing the validity of the map for different working fluids and flow geometries.

As shown in Fig. 13(b), the definition of steady state by the map's authors, in which amplitude of pressure oscillations falls below a certain threshold, does not lend itself well to the present data. Note that the present data superimposed in Fig. 13(b) correspond to vertical upflow and saturated inlet conditions to conform to the map's positive x_e range. For the present data shown, DWOs are present and the flow is unstable in the present definition of flow stability. While this map does rely on dimensionless coordinates, it is not able to predict stability behavior of the present study. Additionally, this map cannot be used with negative x_e values and therefore cannot be assessed for a large fraction of the present data.

A more common approach to developing stability maps is shown in Fig. 14(a)-(c), where phase change number,

$$N_{pch} = \frac{Q}{\dot{m}\,h_{fg}}\,\frac{v_g - v_f}{v_f},$$
(3)

and subcooling number,

$$N_{sub} = \frac{h_f - h_{in}}{h_{fg}}\,\frac{v_g - v_f}{v_f},$$
(4)

are used as x and y coordinates, respectively. By expressing coordinates in terms of dimensionless parameters, these maps allow for better comparison of results across working fluids and geometries.

Fig. 14(a) shows one of the earliest stability maps presented in literature, created by Ishii and Zuber [55] to evaluate experimental data obtained by Solberg [60]. Ishii and Zuber approached the problem of stability by first generating a two-phase flow model, solving the model numerically for a given set of experimental operating conditions, and defining the transition to instability as a point at which low frequency flow oscillations appear.
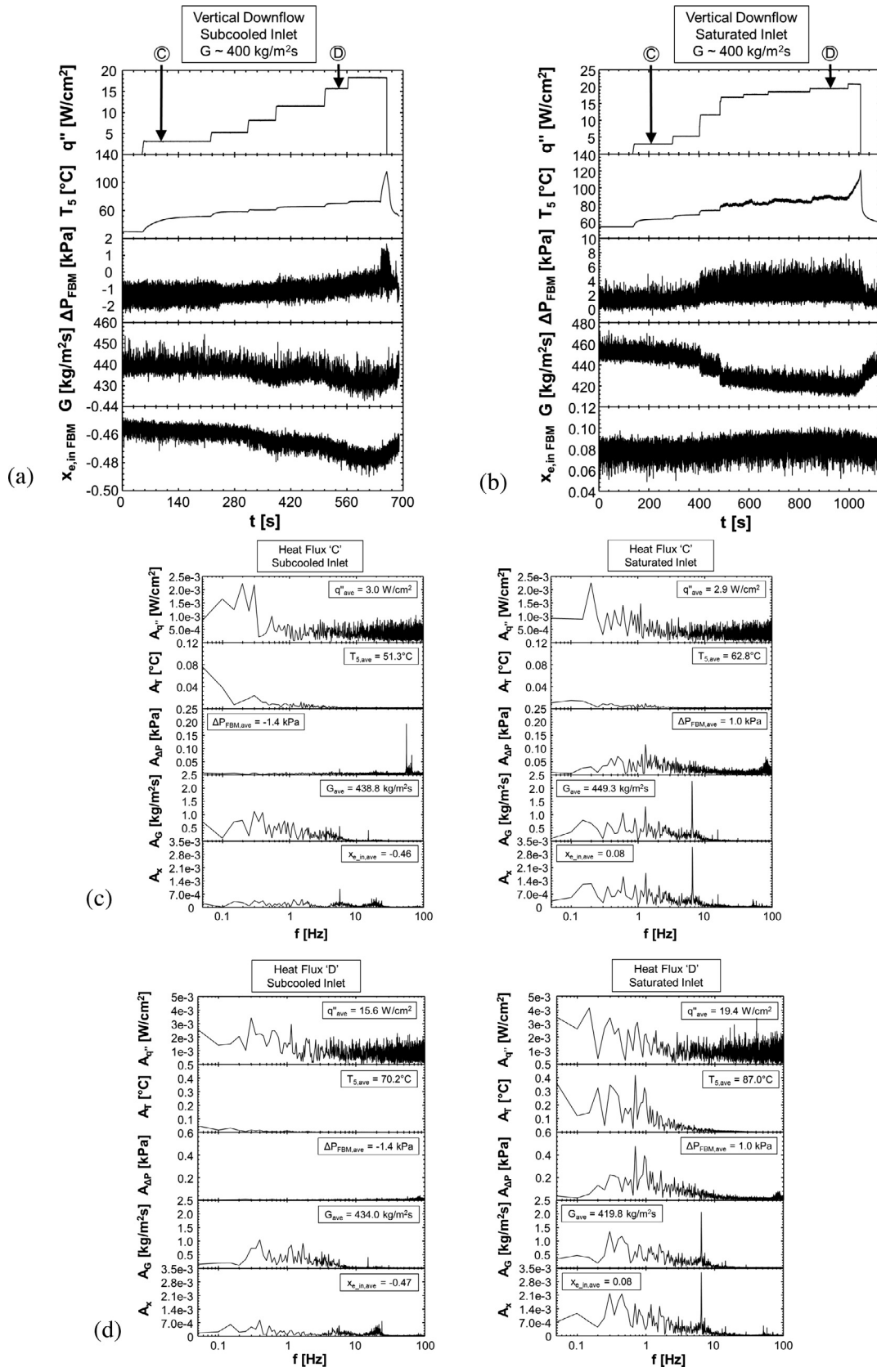
Fig. 11. Transient results for vertical downflow with (a) highly subcooled and (b) saturated inlet conditions. Fast Fourier transforms of key steady-state parameters corresponding to heat fluxes levels 'C' and 'D' for each are compared in (c) and (d).
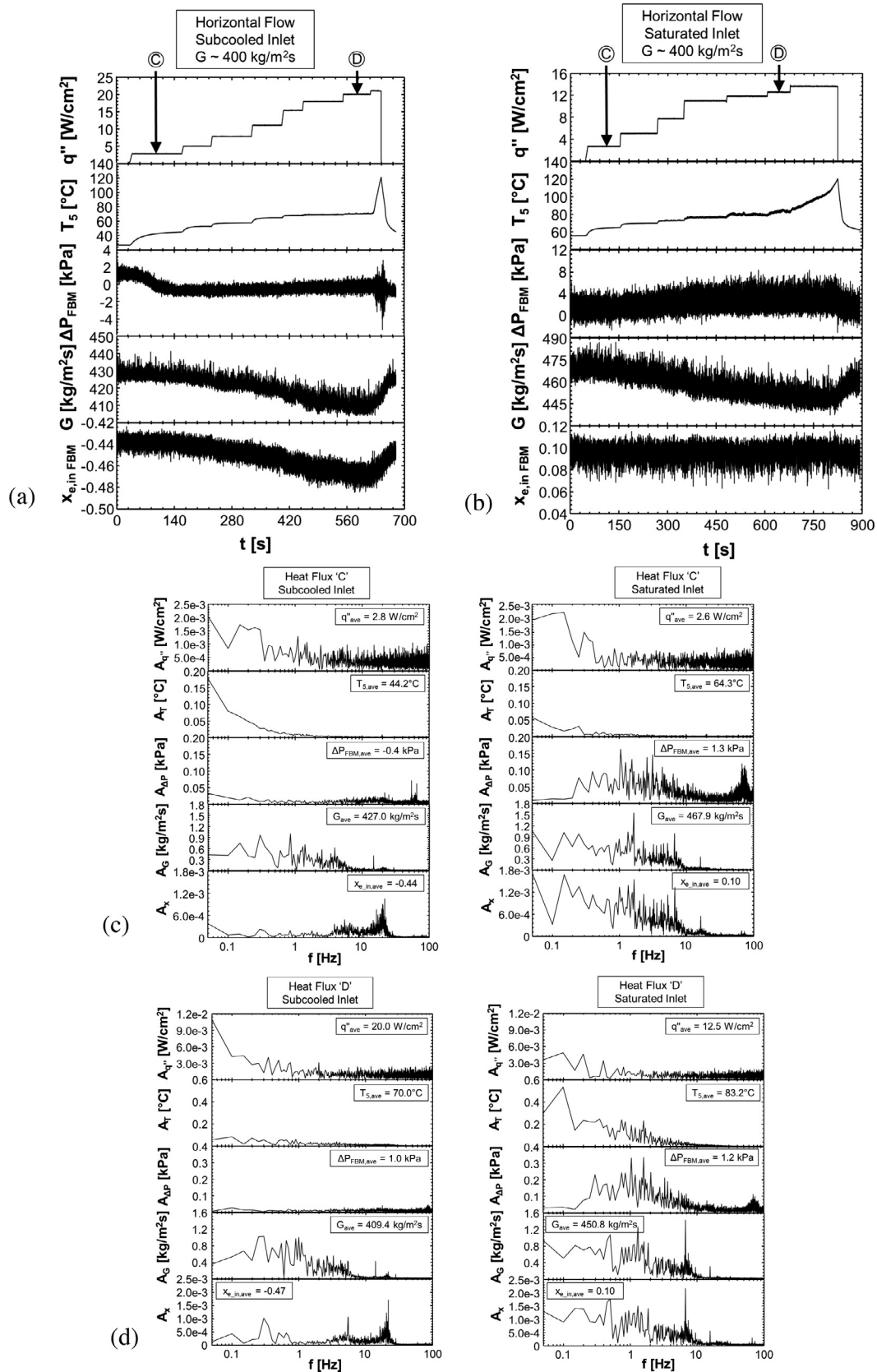
Fig. 12. Transient results for horizontal flow with (a) highly subcooled and (b) saturated inlet conditions. Fast Fourier transforms of key steady-state parameters corresponding to heat fluxes levels 'C' and 'D' for each are compared in (c) and (d).

Table 4
Description of works on which stability maps are based.

Authors	Working fluid	Hydraulic diameter [mm]	Mass velocity [kg/m² s]	Heat flux [kW/m²]	Test section configuration	Stability map coordinates	Concept of stability
Ishii and Zuber [55]	Analytic investigation				Single circular mini-channel	N_{sub} vs. N_{pch}	– Instability identified by existence of low frequency flow oscillations within system – Evaluated using data of Solberg [60] for flow boiling of water in 5.25-mm diameter tub
Lee and Pan [56]	Analytic investigation				Single micro-channel, parallel micro-channels	N_{sub} vs. N_{pch}	– Cases with no oscillations or with finite amplitude oscillations (termed 'Limit Cycle Oscillations' by the original authors) identified as stable – Instability identified by exponential increase in amplitude of oscillations
Brutin and Tadrist [57]	n-pentane	0.889	~10–2500	15.7–125.6	Single micro-channel	$x_{e,out}$ vs. $Re_{f,in}$	– Instability identified by large amplitude pressure drop fluctuations – Threshold for amplitude evaluated empirically
Chang and Pan [58]	Water	0.0863	22–110	7.68–87.7	15 parallel micro-channels	N_{sub} vs. N_{pch}	– Parallel channel instability identified by pressure drop fluctuations of $\Delta P_{max} - \Delta P_{min} > 6$ kPa
Bogojevic et al. [59]	Water	0.194	72.2–433.3	178–445	40 parallel micro-channels	q'' vs. G	– High-Amplitude, Low Frequency (HALF) oscillations, and Low-Amplitude, High Frequency (LAHF) oscillations – Stability implies absence of both oscillation types
Present Study	FC-72	3.33	176.5–2442.5	0–547	Single rectangular channel	N_{sub} vs. N_{pch}	– Stability implies inexistence of DWOs – Instability based on existence of DWOs

Fig. 14(b) shows the stability map generated by Lee and Pan [56] to detail numeric stability of the solution for flow in a micro-channel. It is worth noting that the 'unstable' region corresponds to conditions where amplitude of oscillations increases exponentially, while the 'stable' region encompasses both flow without oscillations and flow with finite amplitude oscillations (termed 'limit cycle oscillations' by Lee and Pan), of which DWOs are a subset.

Fig. 14(c) shows the map of Chang and Pan [58], which is based on experimental data obtained for subcooled flow boiling in a micro-channel heat sink. They identified the onset of parallel channel instability as the point at which pressure oscillations within the micro-channel heat sink reach sufficient magnitude to initiate backflow in some channels. They also used data gathered by Qu and Mudawar [35] to validate their stability boundary, making it one of the stronger tools available for prediction of operating conditions for which parallel channel instability will manifest.

Unfortunately, the three stability maps in Fig. 14 do not lend themselves well to application using the present data, where physical instabilities are encountered exclusively for saturated inlet conditions, which correspond to negative values of N_{sub}. For this reason, expanded stability maps are needed which can encompass test cases corresponding to saturated flow boiling.

5.2. New qualitative stability maps for density wave oscillations

As mentioned above, stability maps are inherently tied to the concept of stability used by their creators, meaning application of stability maps has little utility unless concepts of 'stability' and 'instability' are clearly defined. In the present study, 'instability' will be defined as conditions under which DWOs are observed within the system, while 'stability' is considered the absence of DWO induced behavior.

Fig. 15(a), (b), and (c) show stability maps for vertical upflow, vertical downflow, and horizontal flow orientations. In each case, there is a clear boundary between subcooled flow boiling (associated with positive values of N_{sub}) and saturated flow boiling (associated with negative values of N_{sub}). Also, the range of N_{pch} varies significantly across orientations, with Fig. 15(a) showing vertical upflow reaching peak values of $N_{pch} > 50$, while Fig. 15(b) and (c) show values of $N_{pch} < 35$.

Also indicated on each plot is a qualitative boundary line, summarizing trends seen regarding the existence of DWOs for different operating conditions in each orientation. The boundary line in Fig. 15(a) illustrates the fact that DWOs are present for even the lowest mass velocities (i.e., highest phase change numbers) tested in vertical upflow orientation, apparent in the lack of concavity in the boundary line at high values of N_{pch} (i.e., low values of mass velocity). The boundary line also indicates the necessity of saturated flow conditions for the occurrence of DWOs, evidenced by it's position near $N_{sub} = 0$.

Fig. 15(b) shows how, even for saturated inlet conditions, a threshold mass velocity is required for the formation of DWOs in vertical downflow. This is represented by the downward pointing boundary line for high phase change numbers, which represent relatively low mass flowrates present in the denominator of Eq. (3). For horizontal flow, Fig. 15(c) presents trends similar to those for vertical downflow.

Although all subplots in Fig. 15 provide relevant information regarding the existence of DWOs in flow boiling, there is room for improvement in the formulation of stability maps depicting the onset of DWOs. Additional tests involving saturated flow boiling at higher mass velocities would provide valuable information and help extend the range of the stability maps presented. Furthermore, by conducting tests along the boundary between observation and non-observation of DWOs within the FBM for each
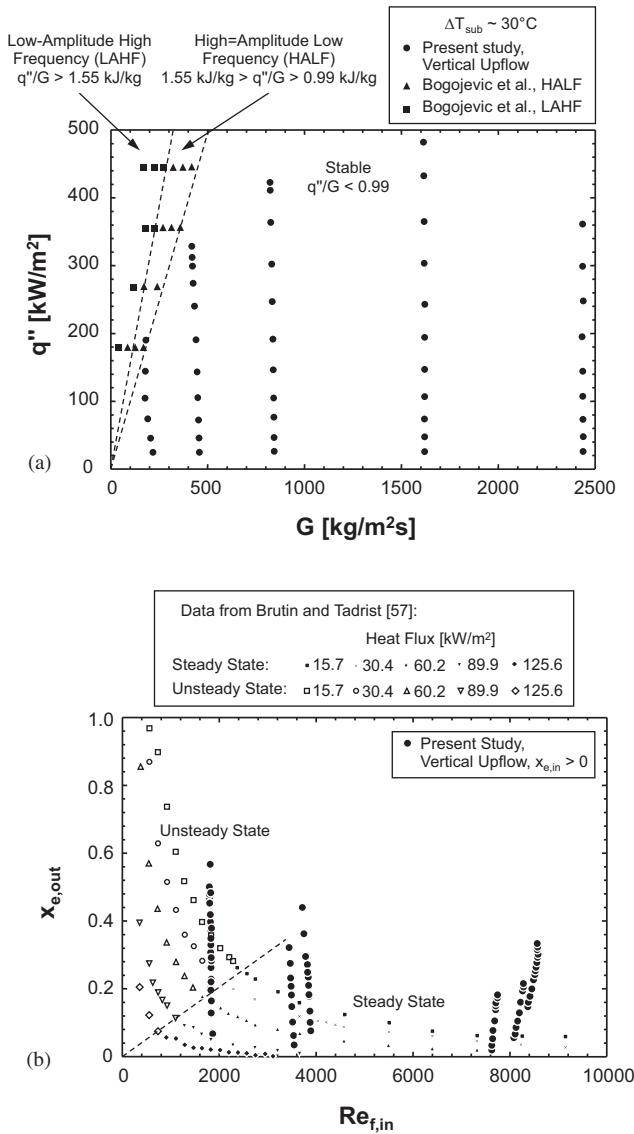
Fig. 13. Data from the present experiments superimposed on stability maps of (a) Bogojevic et al. [59] and (b) Brutin and Tadrist [57].

orientation, the stability boundary could be further refined. Also, by performing similar experiments using different working fluids, predictions could be better generalized to account for variations in key fluid properties such as latent heat of vaporization, phase density difference, and surface tension.

6. Conclusions

This study presented dynamic results for flow boiling of FC-72 in a rectangular channel subjected to heating from two opposite sides. Tests were executed for a range of mass velocities for sub-cooled and saturated inlet conditions in vertical upflow, vertical downflow, and horizontal flow orientations. High frequency pressure measurements made throughout the flow loop were used to assess the influence of individual loop components on the dynamic behavior of the working fluid. By isolating the influence of mechanically induced flow disturbances, physical instability modes were identified and analyzed, primarily within the test section itself. Several stability maps were then presented, with pros and cons of each discussed. Key findings from this study are as follows:
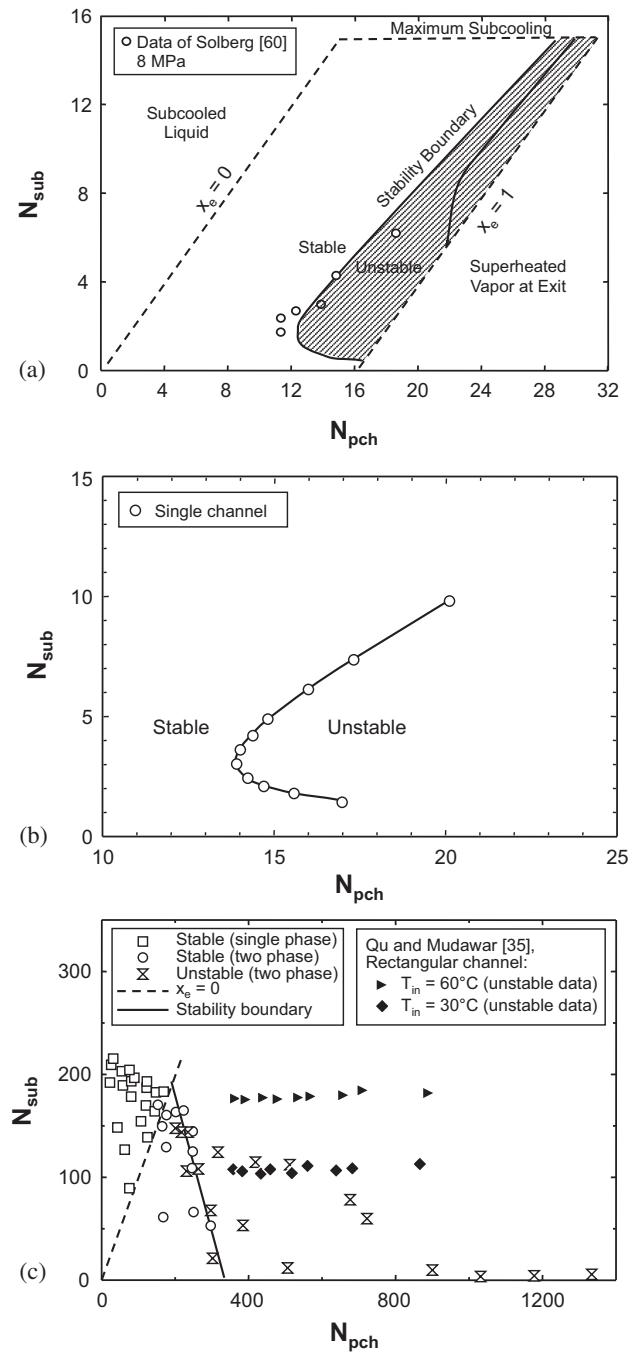
Fig. 14. Flow boiling stability maps adapted from (a) Ishii and Zuber [55], (b) Lee and Pan [56], and (c) Chang and Pan [58].

(1) Analysis of flow dynamic behavior throughout the flow loop revealed that fluctuations within the single-phase liquid regions of the loop are dominated by mechanically induced oscillations, primarily from rotary motion of the pump and vibrations from air fans mounted on the condenser.

(2) Within the two-phase region of the flow loop, pressure fluctuations exhibited characteristics commonly associated with Density Wave Oscillations (DWOs). Flow visualization images were utilized to show that pressure fluctuations representative of DWOs are associated with cyclical passage of High Density and Low Density Fronts through the measurement region. A simple method for prediction of characteristic frequency was put forward, and shown to provide

Fig. 15. Stability maps indicating conditions under which Density Wave Oscillations are present for (a) vertical upflow, (b) vertical downflow, and (c) horizontal flow orientations.

presented that provide qualitative information regarding the conditions for which DWOs form in vertical upflow, vertical downflow, and horizontal flow orientations.

Conflict of interest

The authors declare that there are no conflicts of interest.

Acknowledgements

Appendix A. Supplementary material

Supplementary data associated with this article can be found, in the online version, at https://doi.org/10.1016/j.ijheatmasstransfer.2017.12.011.

References

[1] I. Mudawar, Two-phase micro-channel heat sinks: theory, applications and limitations, J. Electronic Packaging – Trans. ASME 133 (2011) 041002-2.
[2] S. Lee, I. Mudawar, M.M. Hasan, Thermal analysis of hybrid single-phase, two-phase and heat pump thermal control system (TCS) for future spacecraft, Appl. Therm. Eng. 100 (2016) 190–214.
[3] F.P. Chiramonte, J.A. Joshi, Workshop on Critical Issues in Microgravity Fluids, Transport, and Reaction Processes in Advanced Human Support Technology – Final Report, NASA TM-2004-212940, 2004.
[4] The National Academies, Recapturing a Future for Space Exploration: Life and Physical Sciences Research for a New Era, National Academies Press, Washington, DC, 2011.
[5] P.J. Marto, V.J. Lepere, Pool boiling heat transfer from enhanced surfaces to dielectric fluids, J. Heat Transf. – Trans. ASME 104 (1982) 292–299.
[6] I. Mudawar, T.M. Anderson, Parametric investigation into the effects of pressure, subcooling, surface augmentation and choice of coolant on pool boiling in the design of cooling systems for high-power density chips, J. Electronic Packaging - Trans. ASME 112 (1990) 375–382.
[7] J.A. Shmerler, I. Mudawar, Local heat transfer coefficient in wavy free-falling turbulent liquid films undergoing uniform sensible heating, Int. J. Heat Mass Transf. 31 (1988) 67–77.
[8] J.A. Shmerler, I. Mudawar, Local evaporative heat transfer coefficient in turbulent free-falling liquid films, Int. J. Heat Mass Transf. 31 (1988) 731–742.
[9] T.H. Lyu, I. Mudawar, Statistical investigation of the relationship between interfacial waviness and sensible heat transfer to a falling liquid film, Int. J. Heat Mass Transf. 34 (1991) 1451–1464.
[10] K.E. Gungor, R.H.S. Winterton, General correlation for flow boiling in tubes and annuli, Int. J. Heat Mass Transf. 29 (1986) 351–358.
[11] H.J. Lee, S.Y. Lee, Heat transfer correlation for boiling flows in small rectangular horizontal channels with low aspect ratios, Int. J. Multiphase Flow 27 (2001) 2043–2062.
[12] S. Mukherjee, I. Mudawar, Smart pumpless loop for micro-channel electronic cooling using flat and enhanced surfaces, IEEE Trans-CPMT: Components Pack. Technol. 26 (2003) 99–109.
[13] M. Monde, T. Inoue, Critical heat flux in saturated forced convective boiling on a heated disk with multiple impinging jets, J. Heat Transf. – Trans. ASME 113 (1991) 722–727.
[14] D.C. Wadsworth, I. Mudawar, Enhancement of single-phase heat transfer and critical heat flux from an ultra-high-flux simulated microelectronic heat source to a rectangular impinging jet of dielectric liquid, J. Heat Transf. – Trans. ASME 114 (1992) 764–768.
[15] M.E. Johns, I. Mudawar, An ultra-high power two-phase jet-impingement avionic clamshell module, J. Electronic Packaging – Trans. ASME 118 (1996) 264–270.
[16] D.D. Hall, I. Mudawar, Experimental and numerical study of quenching complex-shaped metallic alloys with multiple, overlapping sprays, Int. J. Heat Mass Transf. 38 (1995) 1201–1216.
[17] L. Lin, R. Ponnappan, Heat transfer characteristics of spray cooling in a closed loop, Int. J. Heat Mass Transf. 46 (2003) 3737–3746.
[18] M. Visaria, I. Mudawar, Effects of high subcooling on two-phase spray cooling and critical heat flux, Int. J. Heat Mass Transf. 51 (2008) 5269–5278.
[19] M.K. Sung, I. Mudawar, Experimental and numerical investigation of single-phase heat transfer using a hybrid jet-impingement/micro-channel cooling scheme, Int. J. Heat Mass Transf. 49 (2006) 682–694.

moderately good capability, but future work to include the influence of body force on prediction of DWO frequency is needed.

(3) Within the test section, cases involving saturated flow boiling displayed strong influence of DWOs on not only pressure, but also key parameters such as heated wall temperature, mass flowrate, and inlet quality. Under conditions where amplitude of DWOs is large, this indicates a capacity for stability considerations to impact cooling system design.

(4) Several stability maps commonly found in the literature were presented and shown to have limited applicability to the present data. Three new stability maps were also

[20] H. Zhang, I. Mudawar, M.M. Hasan, Flow boiling CHF in microgravity, Int. J. Heat Mass Transf. 48 (2005) 3107–3118.

[21] H. Zhang, I. Mudawar, M.M. Hasan, Application of flow boiling for thermal management of electronics in microgravity and reduce-gravity space systems, IEEE Trans. – CPMT: Components Packaging Technol. 32 (2009) 466–477.

[22] M. Ledinegg, Instability of flow during natural and forced circulation, Die Wärme 61 (1938) 891–898.

[23] P. Saha, M. Ishii, N. Zuber, An experimental investigation of the thermally induced flow oscillations in two-phase systems, J. Heat Transf. - Trans. ASME 98 (1976) 616–622.

[24] R.W. Lyczkowski, D. Gidaspow, C.W. Solbrig, E.D. Hughes, Characteristics and stability analyses of transient one-dimensional two-phase flow equations and their finite difference approximations, Nucl. Sci. Eng. 66 (1978) 378–396.

[25] K. Fukuda, S. Hasegawa, Analysis on two-phase flow instability in parallel multichannels, J. Nucl. Sci. Technol. 16 (1979) 190–199.

[26] G. Yadigaroglu, A.E. Bergles, Fundamental and higher-mode density-wave oscillations in two-phase systems, J. Heat Transf. - Trans. ASME 94 (1972) 189–195.

[27] K. Fukuda, T. Kobori, Classification of two-phase flow instability by density wave oscillation model, J. Nucl. Sci. Technol. 16 (1979) 95–108.

[28] J.A. Boure, A.E. Bergles, L.S. Tong, Review of two-phase flow instability, Nucl. Eng. Des. 25 (1973) 165–192.

[29] D.F. Delmastro, A. Clausse, J. Converti, The influence of gravity on the stability of boiling flows, Nucl. Eng. Des. 127 (1991) 129–139.

[30] W.R. Schlichting, R.T. Lahey Jr., M.Z. Podowski, An analysis of interacting instability modes, in a phase change system, Nucl. Eng. Des. 240 (2010) 3178–3201.

[31] L.E. O'Neill, C.R. Kharangate, I. Mudawar, Time-averaged and transient pressure drop for flow boiling with saturated inlet conditions, Int. J. Heat Mass Transf. 103 (2016) 133–153.

[32] C.A. Chen, T.F. Lin, W.-M. Yan, Time periodic saturated flow boiling heat transfer of R-134a in a narrow annular duct due to heat flux oscillation, Int. J. Heat Mass Transf. 106 (2017) 35–46.

[33] C. Huh, J. Kim, M.H. Kim, Flow pattern transition instability during flow boiling in a single microchannel, Int. J. Heat Mass Transf. 50 (2007) 1049–1060.

[34] J. Barber, K. Sefiane, D. Brutin, L. Tadrist, Hydrodynamics and heat transfer during flow boiling instabilities in a single microchannel, Appl. Therm. Eng. 29 (2009) 1299–1308.

[35] W. Qu, I. Mudawar, Measurement and prediction of pressure drop in two-phase micro-channel heat sinks, Int. J. Heat Mass Transf. 46 (2003) 2737–2753.

[36] G. Wang, P. Cheng, H. Wu, Unstable and stable flow boiling in parallel microchannels and in a single microchannel, Int. J. Heat Mass Transf. 50 (2007) 4297–4310.

[37] G. Wang, P. Cheng, A.E. Bergles, Effects of inlet/outlet configurations on flow boiling instability in parallel microchannels, Int. J. Heat Mass Transf. 51 (2008) 2267–2281.

[38] H. Lee, I. Park, I. Mudawar, M.M. Hasan, Micro-channel evaporator for space applications – 1. Experimental pressure drop and heat transfer results for different orientations in earth gravity, Int. J. Heat Mass Transf. 77 (2014) 1213–1230.

[39] S. Lee, I. Mudawar, Transient characteristics of flow boiling in large micro-channel heat exchangers, Int. J. Heat Mass Transf. 103 (2016) 186–202.

[40] S. Lee, I. Mudawar, Thermal and thermodynamic performance, and pressure oscillations of refrigeration loop employing large micro-channel evaporators, Int. J. Heat Mass Transf. 103 (2016) 1313–1326.

[41] L. Tadrist, Review on two-phase flow instabilities in narrow spaces, Int. J. Heat Fluid Flow 28 (2007) 54–62.

[42] S. Kakac, B. Bon, A review of two-phase flow dynamic instabilities in tube boiling systems, Int. J. Heat Mass Transf. 51 (2008) 399–433.

[43] L.C. Ruspini, C.P. Marcel, A. Clausse, Two-phase flow instabilities: a review, Int. J. heat Mass Transf. 71 (2014) 521–548.

[44] S.M. Kim, I. Mudawar, Universal approach to predicting saturated flow boiling heat transfer in mini/micro-channels – Part II. Two-phase heat transfer coefficient, Int. J. Heat Mass Transf. 64 (2013) 1239–1256.

[45] S.M. Kim, I. Mudawar, Theoretical model for local heat transfer coefficient for annular flow boiling in circular mini/micro-channels, Int. J. Heat Mass Transf. 73 (2014) 731–742.

[46] S.M. Kim, I. Mudawar, Review of databases and predictive methods for heat transfer in condensing and boiling mini/micro-channel flows, Int. J. Heat Mass Transf. 77 (2014) 627–652.

[47] C.R. Kharangate, L.E. O'Neill, I. Mudawar, Effects of two-phase inlet quality, mass velocity, flow orientation, and heating perimeter on flow boiling in a rectangular channel: Part 1 – two-phase flow and heat transfer results, Int. J. Heat Mass Transf. 103 (2016) 1261–1279.

[48] S.-M. Kim, I. Mudawar, Universal approach to predicting two-phase frictional pressure drop for adiabatic and condensing mini/micro-channel flows, Int. J. Heat Mass Transf. 55 (2012) 3246–3261.

[49] S.M. Kim, I. Mudawar, Review of databases and predictive methods for pressure drop in adiabatic, condensing and boiling mini/micro-channel flows, Int. J. Heat Mass Transf. 77 (2014) 74–97.

[50] C.R. Kharangate, L.E. O'Neill, I. Mudawar, M.M. Hasan, H.K. Nahra, R. Balasubramaniam, N.R. Hall, A.M. Macner, J.R. Mackey, Effects of subcooling and two-phase inlet on flow boiling heat transfer and critical heat flux in a horizontal channel with one-sided and double-sided heating, Int. J. Heat Mass Transf. 91 (2015) 1187–1205.

[51] C.R. Kharangate, L.E. O'Neill, I. Mudawar, M.M. Hasan, H.K. Nahra, R. Balasubramaniam, N.R. Hall, A.M. Macner, J.R. Mackey, Flow boiling and critical heat flux in horizontal channel with one-sided and double-sided heating, Int. J. Heat Mass Transf. 90 (2015) 323–338.

[52] C.R. Kharangate, C. Konishi, I. Mudawar, Consolidated methodology to predicting flow boiling critical heat flux for inclined channels in Earth gravity and for microgravity, Int. J. Heat Mass Transf. 92 (2016) 467–482.

[53] C.R. Kharangate, L.E. O'Neill, I. Mudawar, Effects of two-phase inlet quality, mass velocity, flow orientation, and heating perimeter on flow boiling in a rectangular channel: Part 2 – CHF experimental results and model, Int. J. Heat Mass Transf. 103 (2016) 1280–1296.

[54] R.T. Lahey Jr., M.Z. Podowski, On the analysis of various instabilities in two-phase flow, Multiphase Sci. Technol. 4 (1989) 183–370.

[55] M. Ishii, N. Zuber, Thermally induced flow instabilities in two-phase mixtures, in: Proc. 4th Int. Heat Transfer conf. on Heat Transfer, Paris, vol. 5, paper B5.11, 1970.

[56] J.D. Lee, C. Pan, Dynamics of multiple parallel boiling channel systems with forced flows, Nucl. Eng. Des. 192 (1999) 31–44.

[57] D. Brutin, L. Tadrist, Pressure drop and heat transfer analysis of flow boiling in a minichannel: influence of the inlet condition on two-phase flow stability, Int. J. Heat Mass Transf. 47 (2004) 2365–2377.

[58] K.H. Chang, C. Pan, Two-phase flow instability for boiling in a microchannel heat sink, Int. J. Heat Mass Transf. 50 (2007) 2078–2088.

[59] D. Bogojevic, K. Sefiane, A.J. Walton, H. Lin, G. Cummins, Two-phase flow instabilities in a silicon microchannels heat sink, Int. J. Heat Fluid Flow 30 (2009) 854–867.

[60] K. Solberg, Resulats des essaisd' instabilities sur la boucle 'culine' et comparisons avec un code de calcul, C.E.N.G., Note 225, Centre d'Etudes Nucleaires de Grenoble, France, 1966.